Branching ratios and CP-violating asymmetries of $B_s \rightarrow h_1 h_2$ decays in the general two-Higgs-doublet models

Dong Zhang, Zhenjun Xiao,* and Chong Sheng Li†
Department of Physics, Peking University, Beijing 100871, People's Republic of China
(Received 5 December 2000; published 30 May 2001)

Based on the low-energy effective Hamiltonian with generalized factorization, we calculate the new physics contributions to branching ratios and CP-violating asymmetries of the charmless hadronic decays $B_s \rightarrow h_1 h_2$ in the standard model and the general two-Higgs-doublet models (models I, II, and III). Within the considered parameter space, we find the following. (a) In models I and II, the new physics corrections are always small in size and will be masked by other larger known theoretical uncertainties. (b) In model III, the new physics corrections to the branching ratios of those QCD penguin-dominated decays $\overline{B}_s \rightarrow K^0 \eta^{(\prime)}, K^+ K^{-*}$, etc., are large in size and insensitive to the variations of M_{H^+} and $N_c^{\rm eff}$. For tree- or electroweak penguin-dominated decay modes, however, the new physics corrections are very small in size. (c) For $\overline{B}_s \rightarrow K^+ K^{-*}$ and the other seven decay modes, the branching ratios are at the level of $(1-3) \times 10^{-5}$ and will be measurable at future hadron colliders with large b production. (d) Among the studied 39 B_s meson decay modes, seven of them can have a CP-violating asymmetry $\mathcal{A}_{CP}$ larger than 20% in magnitude. The new physics corrections are small or moderate in magnitude. (e) Because of its large and $N_c^{\rm eff}$ stable branching ratio and CP-violating asymmetry, the decay $\overline{B}_s \rightarrow K^+ K^{-*}$ seems to be the ''best'' channel to find CP violation of B_s system through studies of two-body charmless decays of the B_s meson.

DOI: 10.1103/PhysRevD.64.014014 PACS number(s): 13.25.Hw, 12.15.Ji, 12.38.Bx, 12.60.Fr

I. INTRODUCTION

In B experiments, new physics beyond the standard model (SM) may manifest itself, for example, in the following two ways [1,2]: (a) decays which are expected to be rare in the SM are found to have large branching ratios; (b) CP-violating asymmetries which are expected to vanish or be very small in the SM are found to be significantly large or with a very different pattern than what is predicted in the SM. These potential deviations may be induced by the virtual effects of new physics through loop diagrams.

The observation of many two-body charmless hadronic $B_{u,d}$ meson decays by CLEO, BaBar, and Belle [3–7], the successful start of the asymmetric B factories at SLAC and KEK, and the expectation for a large number of events of $B_{u,d}$ meson decays to be accumulated at B factories and other hadron colliders stimulated intensive investigations of various B decay channels. The two-body charmless hadronic decays $B_{u,d} \rightarrow h_1 h_2$ [where h_1 and h_2 are the light pseudoscalar (P) and/or vector (V) mesons] have been studied, for example, in Refs. [8–13].

It is well known that the low-energy effective Hamiltonian is the basic tool to calculate the branching ratios and $\mathcal{A}_{CP}$ of B meson decays. The short-distance QCD corrected Lagrangian at next leading order (NLO) level is available now [14,15], but we do not know how to calculate the hadronic matrix element from first principles. One conventionally can resort to the factorization approximation [16]. However, we also know that the nonfactorizable contribution really exists and cannot be neglected numerically for most hadronic B decay channels. To remedy the naive factorization hypothesis, some authors [17,10,11] introduced a phenomenological parameter $N_c^{\rm eff}$ (i.e., the effective number of color) to model the nonfactorizable contribution to the hadronic matrix element, which is commonly called the generalized factorization. Very recently, Cheng *et al.* [18] studied and resolved the controversies on the gauge dependence and infrared singularity of the effective Wilson coefficients C_i^{eff} [19] by using the perturbative QCD factorization theorem.

Unlike the $B_{u,d}$ meson, the heavier B_s meson cannot be produced by the Cornell Electron Storage Ring (CESR), KEKB, and PEP-II SLAC e^+e^- storage ring. Only upper limits on the decay rates of several charmless hadronic B_s decays are currently available from the CERN e^+e^- collider LEP collaborations [20,21], such as $B_s \rightarrow K^+K^-$, $K^+\pi^-$, $\pi^0\eta$, and $B_s \rightarrow \eta\eta$, while most of them are far beyond the theoretical predictions. However, it is expected that many B_s decays can be seen at future hadron colliders with large b production. Recent theoretical studies and experimental measurements about the mixing of $B_s^0 - \overline{B}_s^0$ can be found in Refs. [22,23]. Early studies of two-body charmless hadronic decays of B_s mesons can be found in Refs. [24,25]. Based on the framework of generalized factorization, Tseng [26] analyzed the exclusive charmless B_s decays involving $\eta^{(\prime)}$, while Chen, Cheng, and Tseng [12] calculated the branching ratios of 39 charmless two-body decays of B_s mesons. It is found that the branching ratios of $\eta\eta^{(\prime)}$ and several other decay modes can be as large as 10^{-5} and measurable at future experiments.

In a recent work [27], we made a systematic study of the new physics contributions to the branching ratios of 76 $B_{u,d} \rightarrow h_1 h_2$ decay channels in the framework of general two-Higgs-doublet models (2HDMs). In this paper we extend the work to the case of B_s mesons. In addition to the

*Email address: zxiao@ibm320h.phy.pku.edu.cn
†Email address: csli@ibm320h.phy.pku.edu.cn

branching ratios, we here also calculate the new physics contributions to the CP-violating asymmetries A_{CP} of charmless hadronic decays $B_s \to h_1 h_2$ induced by the new gluonic and electroweak charged-Higgs-boson penguin diagrams in the general 2HDMs (models I, II, and III). Using the effective Hamiltonian with improved generalized factorization [18], we evaluate analytically all new strong and electroweak penguin diagrams induced by exchanges of charged Higgs bosons in the quark level processes $b \to qV^*$ with $q \in \{d,s\}$ and $V \in \{\text{gluon}, \gamma, Z\}$, and then combine the new physics contributions with their SM counterparts and finally calculate the branching ratios and CP-violating asymmetries for all 39 exclusive $B_s \to h_1 h_2$ decay modes.

This paper is organized as follows. In Sec. II, we describe the basic structures of the 2HDMs and examine the allowed parameter space of the general 2HDMs from currently available data. In Sec. III, we evaluate analytically the new penguin diagrams and find the effective Wilson coefficients C_i^{eff} with the inclusion of new physics contributions, and present the formulas needed to calculate the branching ratios $\mathcal{B}(B \to h_1 h_2)$. In Secs. IV and V, we calculate and show numerical results of branching ratios and CP-violating asymmetries for 39 B_s decay modes, respectively. We focus on those decay modes with large branching ratios and large CP-violating asymmetries. The conclusions and discussions are included in the final section.

II. GENERAL 2HDMs AND EXPERIMENTAL CONSTRAINTS

The simplest extension of the SM is the so-called two-Higgs-doublet models [28]. In such models, tree level flavor changing neutral current (FCNCs) is absent if one introduces a discrete symmetry to constrain the 2HDM scalar potential and Yukawa Lagrangian. Let us consider a Yukawa Lagrangian of the form [29]

$$\mathcal{L}_Y = \eta_{ij}^U \overline{Q}_{i,L} \widetilde{\phi_1} U_{j,R} + \eta_{ij}^D \overline{Q}_{i,L} \phi_1 D_{j,R} + \xi_{ij}^U \overline{Q}_{i,L} \widetilde{\phi_2} U_{j,R} + \xi_{ij}^D \overline{Q}_{i,L} \phi_2 D_{j,R} + \text{H.c.}, \tag{1}$$

where ϕ_i $(i=1,2)$ are the two Higgs doublets of a two-Higgs-doublet model, $\widetilde{\phi}_{1,2} = i\tau_2 \phi_{1,2}^*$, $Q_{i,L}$ $(U_{j,R})$ with $i=(1,2,3)$ are the left-handed isodoublet quarks (right-handed up-type quarks), and $D_{j,R}$ are the right-handed isosinglet down-type quarks, while $\eta_{i,j}^{U,D}$ and $\xi_{i,j}^{U,D}$ $(i,j=1,2,3$ are family index) are generally the nondiagonal matrices of the Yukawa coupling. By imposing the discrete symmetry $\phi_1 \to -\phi_1$, $\phi_2 \to \phi_2$, $D_i \to -D_i$, and $U_i \to \mp U_i$, one obtains the so-called model I and model II.

During recent years, models I and II have been studied extensively in the literature and tested experimentally, and model II has been very popular since it is the building block of the minimal supersymmetric standard model. In this paper, we focus on the third type of the two-Higgs-doublet model [30], usually known as model III [29,30]. In model III, no discrete symmetry is imposed and both up- and down-type quarks then may have diagonal and/or flavor changing couplings with ϕ_1 and ϕ_2. As described in [29], one can choose a suitable basis $(H^0, H^1, H^2, H^{\pm})$ to express two Higgs doublets. The $H^{\pm}$ are the physical charged Higgs boson, H^0 and h^0 are the physical CP-even neutral Higgs boson, and A^0 is the physical CP-odd neutral Higgs boson. After rotation of the quark fields, the Yukawa Lagrangian of quarks are of the form [29],

$$\mathcal{L}_Y^{III} = \eta_{ij}^U \overline{Q}_{i,L} \widetilde{\phi_1} U_{j,R} + \eta_{ij}^D \overline{Q}_{i,L} \phi_1 D_{j,R} + \hat{\xi}_{ij}^U \overline{Q}_{i,L} \widetilde{\phi_2} U_{j,R} + \hat{\xi}_{ij}^D \overline{Q}_{i,L} \phi_2 D_{j,R} + \text{H.c.}, \tag{2}$$

where $\eta_{ij}^{U,D}$ correspond to the diagonal mass matrices of up- and down-type quarks, while the neutral and charged flavor changing couplings will be [29]. We make the same ansatz on the $\xi_{ij}^{U,D}$ couplings as Ref. [29]:

$$\xi_{ij}^{U,D} = \frac{\sqrt{m_i m_j}}{v} \lambda_{ij}, \quad \hat{\xi}_{neutral}^{U,D} = \xi^{U,D},$$

$$\hat{\xi}_{charged}^U = \xi^U V_{CKM}, \quad \hat{\xi}_{charged}^D = V_{CKM} \xi^D, \tag{3}$$

where V_{CKM} is the Cabibbo-Kobayashi-Maskawa mixing matrix [31], and $i,j=(1,2,3)$ are the generation index. The coupling constants λ_{ij} are free parameters to be determined by experiments, and they may also be complex.

In model II and setting $1 \leqslant \tan\beta = v_2/v_1 \leqslant 50$ favored by experimental measurements [20], the constraint on the mass of charged Higgs boson due to the CLEO data of $b \to s\gamma$ is $M_{H^+} \geqslant 200$ GeV at the NLO level [32]. For model I, however, the limit can be much weaker due to the possible destructive interference with the SM amplitude. For model III, the situation is not as clear as model II because there are more free parameters here [29,33]. In a recent paper [34], Chao *et al.* studied the decay $b \to s\gamma$ by assuming that only the couplings $\lambda_{tt} = |\lambda_{tt}| e^{i\theta_t}$ and $\lambda_{bb} = |\lambda_{bb}| e^{i\theta_b}$ are nonzero. They found that the constraint on M_{H^+} imposed by the CLEO data of $b \to s\gamma$ can be greatly relaxed by considering the phase effects of λ_{tt} and λ_{bb}. From the studies of Refs. [34,35], we know that for model III the parameter space

$$\lambda_{ij} = 0, \quad \text{for} \quad ij \neq tt \quad \text{or} \quad bb,$$

$$|\lambda_{tt}| = 0.3, \quad |\lambda_{bb}| = 35, \quad \theta = (0° - 30°),$$

$$M_{H^+} = (200 \pm 100) \ \text{GeV}, \tag{4}$$

are allowed by the available data, where $\theta = \theta_{bb} - \theta_{tt}$.

From the CERN e^+e^- collider (LEP) and the Fermilab Tevatron searches for charged Higgs bosons [36], the new combined constraint in the $(M_{H^+} - \tan\beta)$ plane has been given, for example, in Ref. [20]: the direct lower limit is $M_{H^+} > 77$ GeV, while $0.5 \leqslant \tan\beta \leqslant 60$ for a relatively light charged Higgs boson with $M_{H^+} \sim 100$ GeV. Combining the direct and indirect limits together, we here conservatively consider the range of 100 GeV $\leqslant M_{H^+} \leqslant 300$ GeV, while take $M_{H^+} = 200$ GeV as the typical value for models I, II, and III. For models I and II we consider the range of $1 \leqslant \tan\beta \leqslant 50$, while take $\tan\beta = 2$ as the typical value.

III. EFFECTIVE HAMILTONIAN IN THE SM AND 2HDMs

The standard theoretical frame to calculate the inclusive three-body decays $b\to s\bar{q}q$[1] is based on the effective Hamiltonian [15,11,13]

$$\mathcal{H}_{eff}(\Delta B=1)=\frac{G_F}{\sqrt{2}}\left\{\sum_{j=1}^{2} C_j(V_{ub}V_{us}^{*}Q_j^{u}+V_{cb}V_{cs}^{*}Q_j^{c}) -V_{tb}V_{ts}^{*}\left[\sum_{j=3}^{10} C_jQ_j+C_gQ_g\right]\right\}. \tag{5}$$

Here the first ten operators Q_1–Q_{10} can be found, for example, in Refs. [11,13,27], while the chromomagnetic operator reads

$$Q_g=\frac{g_s}{8\pi^2}m_b\bar{s}_\alpha\sigma^{\mu\nu}(1+\gamma_5)T^a_{\alpha\beta}b_\beta G^a_{\mu\nu} \tag{6}$$

where α and β are the $SU(3)$ color indices, and $T^a_{\alpha\beta}$ ($a=1,\ldots,8$) are the Gell-Mann matrices. Following Ref. [12], we do not consider the effect of weak annihilation and exchange diagrams.

The coefficients C_i in Eq. (5) are the well-known Wilson coefficient. Within the SM and at scale M_W, the Wilson coefficients $C_1(M_W),\ldots,C_{10}(M_W)$ and $C_g(M_W)$ have been given, for example, in Refs. [14,15]. By using QCD renormalization group equations, it is straightforward to run Wilson coefficients $C_i(M_W)$ from the scale $\mu=0(M_W)$ down to the lower scale $\mu=O(m_b)$. Working consistently to NLO precision, the Wilson coefficients C_i for $i=1,\ldots,10$ are needed in NLO precision, while it is sufficient to use the leading logarithmic value for C_g.

A. New strong and electroweak penguins

For the charmless hadronic decays of B mesons under consideration, the new physics will manifest itself by modifying the corresponding Inami-Lim functions $C_0(x),D_0(x),E_0(x)$, and $E_0'(x)$ which determine the coefficients $C_3(M_W),\ldots,C_{10}(M_W)$ and $C_g(M_W)$. These modifications, in turn, will change the SM predictions of the branching ratios and CP-violating asymmetries for the decays $B_s\to h_1h_2$ under study.

The new strong and electroweak penguin diagrams can be obtained from the corresponding penguin diagrams in the SM by replacing the internal $W^\pm$ lines with the charged-Higgs-boson H^+ lines. In Ref. [27], we calculated analytically the new Z^0-, γ- and gluon-penguin diagrams induced by the exchanges of charged Higgs boson H^+, and found the new C_0,D_0,E_0, and E_0' functions which describe the new physics contributions to the Wilson coefficients through the new penguin diagrams

$$C_0^{III}=\frac{-x_t}{16}\left[\frac{y_t}{1-y_t}+\frac{y_t}{(1-y_t)^2}\ln[y_t]\right]|\lambda_{tt}|^2, \tag{7}$$

$$D_0^{III}=-\frac{1}{3}H(y_t)|\lambda_{tt}|^2, \tag{8}$$

$$E_0^{III}=-\frac{1}{2}I(y_t)|\lambda_{tt}|^2, \tag{9}$$

$$E_0'^{III}=\frac{1}{6}J(y_t)|\lambda_{tt}|^2-K(y_t)|\lambda_{tt}\lambda_{bb}|e^{i\theta}, \tag{10}$$

with

$$H(y)=\frac{38y-79y^2+47y^3}{72(1-y)^3}+\frac{4y-6y^2+3y^4}{12(1-y)^4}\ln[y], \tag{11}$$

$$I(y)=\frac{16y-29y^2+7y^3}{36(1-y)^3}+\frac{2y-3y^2}{6(1-y)^4}\ln[y], \tag{12}$$

$$J(y)=\frac{2y+5y^2-y^3}{4(1-y)^3}+\frac{3y^2}{2(1-y)^4}\ln[y], \tag{13}$$

$$K(y)=\frac{-3y+y^2}{4(1-y)^2}-\frac{y}{2(1-y)^3}\ln[y], \tag{14}$$

where $x_t=m_t^2/M_W^2$, $y_t=m_t^2/M_{H^+}^2$, and the small terms proportional to m_b^2/m_t^2 have been neglected. In models I and II, one can find the corresponding functions C_0, D_0, E_0, and E_0' by evaluating the new strong and electroweak penguin diagrams in the same way as that in model III:

$$C_0^{I}=C_0^{II}=\frac{-x_t}{8\tan^2\beta}\left[\frac{y_t}{1-y_t}+\frac{y_t}{(1-y_t)^2}\ln[y_t]\right], \tag{15}$$

$$D_0^{I}=D_0^{II}=-\frac{2}{3\tan^2\beta}H(y_t), \tag{16}$$

$$E_0^{I}=E_0^{II}=-\frac{1}{\tan^2\beta}I(y_t), \tag{17}$$

$$E_0'^{I}=\frac{1}{3\tan^2\beta}[J(y_t)-6K(y_t)], \tag{18}$$

$$E_0'^{II}=\frac{1}{3\tan^2\beta}J(y_t)+2K(y_t), \tag{19}$$

where $y_t=m_t^2/M_{H^+}^2$, $\tan\beta=v_2/v_1$, and where v_1 and v_2 are the vacuum expectation values of the Higgs doublet ϕ_1 and ϕ_2 as defined before.

[1]For $b\to d\bar{q}q$ decays, one simply makes the replacement $s\to d$.

Combining the SM part and the new physics part together, the NLO Wilson coefficients $C_i(M_W)$ and $C_g(M_W)$ can be written as

$$C_1(M_W)=1-\frac{11}{6}\frac{\alpha_s(M_W)}{4\pi}-\frac{35}{18}\frac{\alpha_{em}}{4\pi}, \tag{20}$$

$$C_2(M_W)=\frac{11}{2}\frac{\alpha_s(M_W)}{4\pi}, \tag{21}$$

$$C_3(M_W)=-\frac{\alpha_s(M_W)}{24\pi}\left[E_0(x_t)+E_0^{NP}-\frac{2}{3}\right]+\frac{\alpha_{em}}{6\pi}\frac{1}{\sin^2\theta_W}[2B_0(x_t)+C_0(x_t)+C_0^{NP}], \tag{22}$$

$$C_4(M_W)=\frac{\alpha_s(M_W)}{8\pi}\left[E_0(x_t)+E_0^{NP}-\frac{2}{3}\right], \tag{23}$$

$$C_5(M_W)=-\frac{\alpha_s(M_W)}{24\pi}\left[E_0(x_t)+E_0^{NP}-\frac{2}{3}\right], \tag{24}$$

$$C_6(M_W)=\frac{\alpha_s(M_W)}{8\pi}\left[E_0(x_t)+E_0^{NP}-\frac{2}{3}\right], \tag{25}$$

$$C_7(M_W)=\frac{\alpha_{em}}{6\pi}\left[4C_0(x_t)+4C_0^{NP}+D_0(x_t)+D_0^{NP}-\frac{4}{9}\right], \tag{26}$$

$$C_8(M_W)=C_{10}(M_W)=0, \tag{27}$$

$$C_9(M_W)=\frac{\alpha_{em}}{6\pi}\left\{4C_0(x_t)+4C_0^{NP}+D_0(x_t)+D_0^{NP}-\frac{4}{9}+\frac{1}{\sin^2\theta_W}[10B_0(x_t)-4C_0(x_t)+4C_0^{NP}]\right\}, \tag{28}$$

$$C_g(M_W)=-\frac{1}{2}(E_0'(x_t)+E'^{NP}_0), \tag{29}$$

where $x_t=m_t^2/M_W^2$, and the functions $B_0(x)$, $C_0(x)$, $D_0(x)$, $E_0(x)$, and E_0' are the familiar Inami-Lim functions [37] in the SM and can be found easily, for example, in Refs. [14,38].

Since the heavy new particles appearing in the 2HDMs have been integrated out at the scale M_W, the QCD running of the Wilson coefficients $C_i(M_W)$ down to the scale $\mu=O(m_b)$ after including the new physics contributions will be the same as in the SM:

$$\mathbf{C}(\mu)=U(\mu,M_W)\mathbf{C}(M_W), \tag{30}$$

$$C_g(\mu)=\eta^{14/23}C_g(M_W)+\sum_{i=1}^{8}\overline{h_i}\eta^{a_i}, \tag{31}$$

where $\mathbf{C}(M_W)=[C_1(M_W),\ldots,C_{10}(M_W)]^T$, $U(\mu,M_W)$ is the five-flavor 10×10 evolution matrix at NLO level as defined in Ref. [14], $\eta=\alpha_s(M_W)/\alpha_s(\mu)$, and the constants $\overline{h_i}$ and a_i can also be found in Ref. [14].

In the naive dimensional reduction (NDR) scheme and for $SU(3)_C$, the effective Wilson coefficients[2] can be written as [13]

$$C_i^{eff}=\left[1+\frac{\alpha_s}{4\pi}\left(\hat{r}_V^T+\gamma_V^T\log\frac{m_b}{\mu}\right)\right]_{ij}C_j+\frac{\alpha_s}{24\pi}A_i'(C_t+C_p+C_g)+\frac{\alpha_{ew}}{8\pi}B_i'C_e, \tag{32}$$

where

$$A_i'=(0,0,-1,3,-1,3,0,0,0,0)^T,$$

$$B_i'=(0,0,0,0,0,0,1,0,1,0)^T$$

the matrices $\hat{r}_V$ and γ_V contain the process-independent contributions from the vertex diagrams. The matrix γ_V and $\hat{r}_V$ have been given explicitly, for example, in Eqs. (2.17) and (2.18) of Ref. [13]. Note that the correct value of the element $(\hat{r}_{NDR})_{66}$ and $(\hat{r}_{NDR})_{88}$ should be 17 instead of 1 as pointed out in Ref. [39].

The functions C_t, C_p, and C_g describe the contributions arising from the penguin diagrams of the current-current $Q_{1,2}$ and the QCD operators Q_3–Q_6 and the tree-level diagram of the magnetic dipole operator Q_{8G}, respectively. We here also follow the procedure of Ref. [10] to include the contribution of magnetic gluon penguin. The functions C_t, C_p, and C_g are given in the NDR scheme by [11,13]

$$C_t=\left[\frac{2}{3}+\frac{\lambda_u}{\lambda_t}G(m_u)+\frac{\lambda_c}{\lambda_t}G(m_c)\right]C_1, \tag{33}$$

$$C_p=\left[\frac{4}{3}-G(m_q)-G(m_b)\right]C_3+\left[\frac{10}{3}-\sum_{i=u,d,s,c,b}G(m_i)\right](C_4+C_6), \tag{34}$$

$$C_e=\frac{8}{9}\left[\frac{2}{3}+\frac{\lambda_u}{\lambda_t}G(m_u)+\frac{\lambda_c}{\lambda_t}G(m_c)\right](C_1+3C_2), \tag{35}$$

$$C_g=-\frac{2m_b}{\sqrt{\langle k^2\rangle}}C_g^{\rm eff}, \tag{36}$$

with $\lambda_{q'}\equiv V_{q'b}V_{q'q}^*$ and $C_g^{eff}=C_g(\mu)+C_5$. The function $G(m)$ can be found, for example, in Refs. [13,27]. For the two-body exclusive B meson decays any information on k^2 is lost in the factorization assumption; one usually uses the

[2]In the improved generalized factorization approach [18], these effective coefficients are renormalization scale and scheme independent, gauge invariant, and infrared safe.

TABLE I. Numerical values of a_i for the transitions $b \to d$ $[\overline{b} \to \overline{d}]$. The first, second and third entries for $a_3, \ldots, a_{10}$ refer to the values of a_i in the SM and models II and III, respectively. All entries for $a_3, \ldots, a_{10}$ should be multiplied by 10^{-4}.

	$N_c^{\rm eff}=2$	$N_c^{\rm eff}=3$	$N_c^{\rm eff}=\infty$
a_1	0.985 [0.985]	1.046 [1.046]	1.169 [1.169]
a_2	0.216 [0.216]	0.021 [0.021]	−0.369 [−0.369]
a_3	$-10.4-19.1i[-11.5-25.7i]$	66.1 [66.1]	$219+38.1i[221+51.4i]$
	$-33.0-19.1i[-34.1-25.7i]$	66.2 [66.2]	$265+38.1i[267+51.4i]$
a_4	$-349-95.3i[-354-129i]$	$-386-102i[-392-137i]$	$-459-114i[-466-154i]$
	$-463-95.3i[-469-129i]$	$-507-102i[-513-137i]$	$-596-114i[-602-154i]$
a_5	$-163-19.1i$ $[-164-25.7i]$	−61.5 [−61.5]	$142+38.1i[144+51.4i]$
	$-186-19.1i$ $[-187-25.7i]$	−61.4 [−61.4]	$187+38.1i[189+51i.4]$
a_6	$-538-95.3i[-544-129i]$	$-562-102i[-568-137i]$	$-609-114i[-616-154i]$
	$-652-95.3i[-657-129i]$	$-683-102i[-689-137i]$	$-746-114i[-752-154i]$
a_7	$5.2-2.5i[5.1-3.1i]$	$4.1-2.5i[4.0-3.1i]$	$2.1-2.5i[2.0-3.1i]$
	$5.4-2.5i[5.3-3.1i]$	$4.3-2.5i[4.2-3.1i]$	$2.2-2.5i[2.1-3.1i]$
a_8	$7.2-1.3i[7.2-1.6i]$	$6.9-0.8i$ $[6.8-1.0i]$	6.2 [6.2]
	$7.4-1.3i[7.3-1.6i]$	$7.0-0.8i$ $[7.0-1.0i]$	6.3 [6.3]
a_9	$-85.8-2.5i[-85.9-3.1i]$	$-91.7-2.5i[-91.8-3.1i]$	$-103-2.5i[-104-3.1i]$
	$-86.4-2.5i[-86.5-3.1i]$	$-92.3-2.5i[-92.4-3.1i]$	$-104.1-2.5i[-104-3.1i]$
a_{10}	$-16.5-1.3i[-16.6-1.6i]$	$0.7-0.8i[0.7-1.0i]$	35.2 [35.2]
	$-16.6-1.3i[-16.7-1.6i]$	$0.7-0.8i[0.7-1.0i]$	35.4 [35.4]

''physical'' range for k^2 [11–13]: $m_b^2/4 \lesssim k^2 \lesssim m_b^2/2$. Following Refs. [11–13] we take $k^2 = m_b^2/2$ in the numerical calculation.

B. Decay amplitudes in the BSW model

Following Ref. [12], the possible effects of final state interactions (FSIs) and contributions from annihilation channels will be neglected although they may play a significant role for some decay modes. The new physics effects on the B decays under study will be included by using the modified effective coefficients a_i $(i=3,\ldots,10)$ as given in the second entries of Table I and Table II for model III. The effective coefficients a_i in models I and II are not shown explicitly in Table I and Table II. In the numerical calculations the input parameters as given in the Appendix and Eq. (4) will be used implicitly.

TABLE II. Same as Table I but for $b \to s$ $[\overline{b} \to \overline{s}]$ transitions.

	$N_c^{\rm eff}=2$	$N_c^{\rm eff}=3$	$N_c^{\rm eff}=\infty$
a_1	0.985 [0.985]	1.046 [1.046]	1.169 [1.169]
a_2	0.216 [0.216]	0.021 [0.021]	−0.369 [−0.369]
a_3	$-10.9-21.7i[-9.8-22.1i]$	66.1 [66.1]	$220+43.3i[218+44.3i]$
	$-33.6-22.7i[-32.5-22.2i]$	66.2 [66.2]	$266+43.3i[264+44.3i]$
a_4	$-352-108i[-346-111i]$	$-389-116i[-383-118i]$	$-462-130i[-455-133i]$
	$-467-108i[-460-111i]$	$-510-116i[-504-118i]$	$-599-130i[-592-133i]$
a_5	$-164-22.7i[-162-22.2i]$	−61.5 [−61.5]	$143+43.3i[140+44.3i]$
	$-186-21.7i[-185-22.2i]$	−61.4 [−61.4]	$188+43.3i[186+44.3i]$
a_6	$-541-108i[-535-111i]$	$-565-116i[-559-118i]$	$-612-130i[-606-133i]$
	$-654-108i[-649-111i]$	$-686-116i[-680-118i]$	$-749-130i[-742-133i]$
a_7	$5.1-2.8i$ $[5.2-2.8i]$	$4.1-2.8i[4.2-2.8i]$	$2.0-2.8i[2.1-2.8i]$
	$5.3-2.8i$ $[5.4-2.8i]$	$4.3-2.8i[4.4-2.8i]$	$2.2-2.8i[2.3-2.8i]$
a_8	$7.2-1.4i$ $[7.2-1.4i]$	$6.9-0.9i$ $[6.9-0.9i]$	6.2 [6.2]
	$7.4-1.4i$ $[7.4-1.4i]$	$7.0-0.9i$ $[7.0-0.9i]$	6.3 [6.3]
a_9	$-85.9-2.8i[-85.8-2.8i]$	$-91.7-2.8i[-91.6-2.8i]$	$-104-2.8i[-103-2.8i]$
	$-86.5-2.8i$ $[-86.4-2.8i]$	$-92.4-2.8i[-92.3-2.8i]$	$-104-2.8i[-104-2.8i]$
a_{10}	$-16.6-1.4i[-16.5-1.4i]$	$0.7-0.9i$ $[0.7-0.9i]$	35.2 [35.2]
	$-16.7-1.4i[-16.6-1.4i]$	$0.7-0.9i$ $[0.7-0.9i]$	35.4 [35.4]

With the factorization ansatz [16], the three-hadron matrix elements or the decay amplitude $\langle XY|H_{eff}|B_s\rangle$ can be factorized into a sum of products of two current matrix elements $\langle X|J_1^{\mu}|0\rangle$ and $\langle Y|J_{2\mu}|B_s\rangle$ (or $\langle Y|J_1^{\mu}|0\rangle$ and $\langle X|J_{2\mu}|B_s\rangle$). The explicit expressions of matrix elements can be found, for example, in Refs. [16,40].

In the B rest frame, the branching ratios of two-body B meson decays can be written as

$$\mathcal{B}(B_s\to XY)=\tau_{B_s}\frac{|p|}{8\pi M_{B_s}^2}|M(B_s\to XY)|^2 \tag{37}$$

for $B_s\to PP$ decays and

$$\mathcal{B}(B_s\to XY)=\tau_{B_s}\frac{|p|^3}{8\pi M_V^2}|M(B_s\to XY)/(\epsilon\cdot p_B)|^2 \tag{38}$$

for $B_s\to PV$ decays. Here $\tau(B_s^0)=1.493$ ps [20], p_B is the four-momentum of the B meson, M_V and ϵ are the mass and polarization vector of the produced light vector meson, respectively, and $|p|$ is the magnitude of momentum of particle X and Y in the B rest frame:

$$|p|=\frac{1}{2M_B}\sqrt{[M_B^2-(M_X+M_Y)^2][M_B^2-(M_X-M_Y)^2]}. \tag{39}$$

For $B_s\to VV$ decays, the situation is more involved. One needs to evaluate the helicity matrix element $H_\lambda=\langle V_1(\lambda)V_2(\lambda)|H_{eff}|B\rangle$ with $\lambda=0,\pm 1$. The branching ratio of the decay $B\to V_1V_2$ is given in terms of H_λ by

$$\mathcal{B}(B_s\to V_1V_2)=\tau_{B_s}\frac{|p|}{8\pi M_B^2}(|H_0|^2+|H_{+1}|^2+|H_{-1}|^2), \tag{40}$$

where $|p|$ has been given in Eq. (39). The three independent helicity amplitudes H_0, H_{+1}, and H_{-1} can be expressed by three invariant amplitudes a,b,c defined by the decomposition

$$H_\lambda=i\epsilon^{\mu}(\lambda)\,\eta^{\nu}(\lambda)\left[ag_{\mu\nu}+\frac{b}{M_1M_2}p_\mu p_\nu+\frac{ic}{M_1M_2}\epsilon_{\mu\nu\alpha\beta}p_1^{\alpha}p^{\beta}\right], \tag{41}$$

where $p_{1,2}$ and $M_{1,2}$ are the four-momentum and masses of $V_{1,2}$, respectively. $p=p_1+p_2$ is the four-momentum of the B meson, and

$$H_{\pm 1}=a\pm c\sqrt{x^2-1},\quad H_0=-ax-b(x^2-1), \tag{42}$$

$$x=\frac{M_B^2-M_1^2-M_2^2}{2M_1M_2}. \tag{43}$$

For individual decay modes, the coefficients a, b, and c can be determined by comparing the helicity amplitude $H_\lambda=\langle V_1(\lambda)V_2(\lambda)|H_{eff}|B_s\rangle$ with expression (41).

In the generalized factorization approach, the effective Wilson coefficients C_i^{eff} will appear in the decay amplitudes in the combinations

$$a_{2i-1}\equiv C_{2i-1}^{\rm eff}+\frac{C_{2i}^{\rm eff}}{N_c^{\rm eff}},\quad a_{2i}\equiv C_{2i}^{\rm eff}+\frac{C_{2i-1}^{\rm eff}}{N_c^{\rm eff}}\quad (i=1,\dots,5) \tag{44}$$

where the effective number of colors, $N_c^{\rm eff}$, is treated as a free parameter varying in the range of $2\leqslant N_c^{\rm eff}\leqslant\infty$, in order to model the nonfactorizable contribution to the hadronic matrix elements. Although $N_c^{\rm eff}$ can in principle vary from channel to channel, in the energetic two-body hadronic B meson decays, it is expected to be process insensitive as supported by the data [12]. As argued in Ref. [17], $N_c^{\rm eff}(LL)$ induced by the $(V-A)(V-A)$ operators can be rather different from $N_c^{\rm eff}(LR)$ generated by $(V-A)(V+A)$ operators. Since we here focus on the calculation of new physics effects on the studied B meson decays induced by the new penguin diagrams in the two-Higgs-doublet models, we will simply assume that $N_c^{\rm eff}(LL)\equiv N_c^{\rm eff}(LR)=N_c^{\rm eff}$ and consider the variation of $N_c^{\rm eff}$ in the range of $2\leqslant N_c^{\rm eff}\leqslant\infty$. For more details about the cases of $N_c^{\rm eff}(LL)\neq N_c^{\rm eff}(LR)$, one can see, for example, Ref. [12]. We here will not consider the possible effects of FSIs and the contributions from annihilation channels although they may play a significant role for some decay modes.

Using the input parameters as given in the Appendix and assuming $k^2=m_b^2/2$, $M_{H^+}=200$ GeV, the theoretical predictions of effective coefficients a_i are calculated and displayed in Table I and Table II for the transitions $b\to d$ ($\overline{b}\to\overline{d}$) and $b\to s$ ($\overline{b}\to\overline{s}$), respectively. For coefficients $a_3,\dots,a_{10}$, the first and second entries in Tables I and II refer to the values of a_i in the SM and model III, respectively.

Compared with Ref. [12], the effective coefficients a_i given here have two new features.

(i) The effective Wilson coefficients C_i^{eff} here are not only renormalization scale and scheme independent, but also gauge invariant and infrared safe.

(ii) The contribution due to the chromomagnetic dipole operator Q_g has been included here through the function C_g as given in Eq. (36). For the penguin-diagram-dominated decay channels, the operator C_g will play an important role.

(iii) The coefficients a_1 and a_2 remain unchanged in 2HDMs since the new physics considered here does not contribute through tree diagrams.

(iv) The new physics contributions are significant to the coefficients a_4 and a_6, but negligibly small to the coefficients $a_{3,5}$ and a_{7-10}.

All branching ratios here are the averages of the branching ratios of B and anti-B decays. The ratio $\delta\mathcal{B}$ describes the new physics correction on the decay ratio and is defined as

$$\delta\mathcal{B}(B_s\to XY)=\frac{\mathcal{B}(B_s\to XY)^{NP}-\mathcal{B}(B_s\to XY)^{SM}}{\mathcal{B}(B_s\to XY)^{SM}}. \quad (45)$$

IV. BRANCHING RATIOS OF B_s MESON DECAYS

Using the formulas and input parameters as given in the last section and in the Appendix, it is straightforward to find the branching ratios for the 39 $B_s\to PP,PV,VV$ decay channels. In the numerical calculations, we use the decay amplitudes as given in Appendixes A, B, and C of Refs. [12] directly without further discussions about details.

Following Refs. [16,12], the hadronic charmless B meson decays can be classified into six classes: the first and last three classes correspond to the tree-dominated and penguin-dominated amplitudes, respectively.

(i) Class-I and class-II decays are dominated by the external and internal W-emission tree diagrams, respectively. Examples are $\overline{B_s}\to K^+\pi^-,K^0\pi^0, \ldots$.

(ii) Class-III decays: the decays involving both external and internal W emissions. But this class does not exist for the B_s decays.

(iii) Class-IV and class-V decay modes are governed by effective coefficients $a_{4,6,8,10}$ and $a_{3,5,7,9}$, respectively. Examples are $\overline{B_s}\to K^+K^-,\pi\eta^{(\prime)}, \ldots$.

(iv) Class-VI decays involve the interference of class-IV and class-V decays.

In Tables III–VI, we present the numerical results of the branching ratios for the 39 $B_s\to PP,PV,VV$ decays in the framework of the SM and models I, II, and III. Theoretical predictions are made by using the central values of input parameters as given in Eq. (4) and the Appendix, and assuming $A=0.804$, $\lambda=0.22$, $\rho=0.16$, $\eta=0.34$, $M_{H^+}=200$ GeV, $\theta=0°,30°$, $\tan\beta=2$, and $N_c^{\rm eff}=2,3,\infty$ in the generalized factorization approach. The k^2 dependence of the branching ratios is small in the range of $k^2=m_b^2/2\pm 2$ GeV^2 and hence the numerical results are given by fixing $k^2=m_b^2/2$.

The SM predictions for all B_s decay modes as listed in Tables III and IV agree well with those given in Ref. [12]. The effect of changing $\hat{r}_V$ and including the new contribution from the chromomagnetic operator Q_g in the SM is not significant.

For decay modes involving $B_s\to K^*$ or $B_s\to\phi$ transitions, we use two different set of form factors: the Bauer-Stech-Wirbel (BSW) form factor [16] and the light-cone sum rule (LCSR) form factor as given explicitly in the Appendix. For the decay modes $B_s\to\pi^0\phi,\phi\eta',\rho^0\phi,\omega\phi$ and $B_s\to\phi\phi$, the variation of the branching ratios induced by using different set of form factors is about a factor of 2, but small or moderate for all other decay modes.

From numerical results, we see the following general features of new physics corrections.

(i) In model III, the new physics corrections to QCD-penguin-dominated decay modes, such as $B_s\to K^0\eta^{(\prime)}$, $\eta^{(\prime)}\eta^{(\prime)}$, $K^0\overline{K^0}$, etc., are large in size and insensitive to variations of the mass M_{H^+} and $N_c^{\rm eff}$: from 30% to 130% with respect to the SM predictions for both cases of $\theta=0°,30°$. For tree-dominated or electroweak penguin-dominated decay modes, however, the new physics corrections are very small in size: $\delta\mathcal{B}\leqslant 5\%$.

(ii) In models I and II, the new physics corrections to all $B_s\to h_1h_2$ decay modes are always small in size within the considered parameter space: less than 10% and 20% in models I and II, respectively, as shown in Tables V and VI. So small corrections will be masked by other larger known theoretical uncertainties. Variation of $\tan\beta$ in the range of $2\leqslant\tan\beta\leqslant 50$ cannot change this feature.

(iii) In model III, the new gluonic penguins will contribute effectively through the mixing of chromomagnetic operator Q_g with QCD penguin operators Q_3–Q_6, as shown in Eq. (32). The C_g^{eff} will strongly dominate the new physics contributions to B_s meson decays. The branching ratios for all 39 decay modes have a very weak dependence on θ in the range of $0°\leqslant\theta\leqslant 30°$.

As pointed in Refs. [12,41], the decays

$$\overline{B_s}\to\eta\pi,\eta'\pi,\eta\rho,\eta'\rho,\phi\pi,\phi\rho \quad (46)$$

do not receive any QCD penguin contributions, and are predominately governed by a_9 and hence are $N_c^{\rm eff}$ insensitive. In 2HDMs, this remains true because the new physics corrections to the coefficients a_{7-10} are negligibly small as shown in Tables I and II, and therefore, the new physics contributions to these decay modes are also very small: $\leqslant 2\%$. As suggested in Ref. [12], a measurement of these six decay modes can be utilized to fix the parameter a_9. It is clear that the inclusion of new physics contributions in the 2HDMs does not change this picture.

For the decays

$$\overline{B_s}\to\omega\eta,\omega\eta',\phi\eta^{(\prime)},K\phi,K^*\phi,\phi\pi, \quad (47)$$

the SM electroweak penguin corrections are in general as important as QCD penguin effects and very sensitive to $N_c^{\rm eff}$. The new physics corrections to these decay modes in model III also have a strong dependence on the variation of $N_c^{\rm eff}$: $\delta\mathcal{B}=-20\%$–110% for $2\leqslant N_c^{\rm eff}\leqslant\infty$. As illustrated in Fig. 1, for example, the branching ratio of $B_s\to\phi\eta$ decay has a moderate M_{H^+} dependence, but a strong $N_c^{\rm eff}$ dependence. For Figs. 1(a) and 1(b), we set $N_c^{\rm eff}=3$ and $M_{H^+}=200$ GeV, respectively. The four curves correspond to the theoretical predictions in the SM (dotted curve), model II (dot-dashed curve), model III with $\theta=0°$ (solid curve), and $\theta=30°$ (short-dashed curve), respectively.

Among the 39 charmless two-body hadronic B_s decays, we find that only seven (eight) of them have branching ratios at the level of 10^{-5} in the SM (model III):

$$\overline{B_s}\to K^+K^-,K^0\overline{K^0},\eta\eta,\eta'\eta^{(\prime)},K^+\rho,K^{+*}\rho^-,\phi\phi. \quad (48)$$

Among these eight decay modes, the new physics correction to the class-I decay mode $\overline{B_s}\to K^+\rho^-$ and $K^{+*}\rho^-$ are very small, from -2% to 1%. For the remaining six decay modes, the new physics enhancement is significant—from $\sim$50% to $\sim$130%—and insensitive to variation of $N_c^{\rm eff}$. These decay modes will be measurable at the future hadron colliders with large b production [12]. In Figs. 2 and 3, we

TABLE III. $\mathcal{B}(B_s \to h_1, h_2)$ (in units of 10^{-6}) in the SM and model III by using the BSW form factors, and assuming $k^2 = m_b^2/2$, $\rho = 0.16$, $\eta = 0.34$, $M_{H^+} = 200$ GeV, $\theta = 0°$, and $N_c^{\rm eff} = 2, 3, \infty$.

		SM: $\mathcal{B}$			Model III: $\mathcal{B}$ and $\delta\mathcal{B}$ [%]					
Channel	Class	2	3	∞	2	3	∞	2	3	∞
$\overline{B_s} \to K^+ \pi^-$	I	6.33	7.14	8.89	6.52	7.35	9.16	3.1	3.1	3.0
$\overline{B_s} \to K^0 \pi^0$	II	0.19	0.08	0.56	0.24	0.14	0.64	23.8	67.1	14.4
$\overline{B_s} \to K^0 \eta$	VI	0.34	0.31	0.79	0.47	0.46	1.00	38.3	49.9	26.8
$\overline{B_s} \to K^0 \eta'$	VI	0.57	0.51	0.77	0.88	0.84	1.17	53.0	65.6	52.3
$\overline{B_s} \to K^+ K^-$	IV	10.7	11.7	14.0	16.7	18.5	22.3	56.5	57.6	59.4
$\overline{B_s} \to \pi^0 \eta$	V	0.04	0.06	0.11	0.04	0.06	0.11	1.9	1.8	1.3
$\overline{B_s} \to \pi^0 \eta'$	V	0.04	0.06	0.10	0.04	0.06	0.11	1.9	1.8	1.3
$\overline{B_s} \to \eta \eta'$	VI	13.8	15.9	20.5	22.5	25.9	33.4	63.8	63.3	62.6
$\overline{B_s} \to \eta' \eta'$	VI	6.79	7.51	9.08	11.6	12.9	15.7	70.6	71.7	73.4
$\overline{B_s} \to \eta \eta$	VI	6.97	8.37	11.6	10.9	13.0	17.7	56.9	55.3	52.8
$\overline{B_s} \to K^0 \overline{K^0}$	IV	11.4	13.2	17.3	17.6	20.4	26.4	66.2	65.6	64.5
$\overline{B_s} \to K^{*+} \pi^-$	I	4.04	4.56	5.70	4.04	4.56	5.70	0.0	0.0	0.0
$\overline{B_s} \to K^+ \rho^-$	I	14.8	16.7	20.8	14.9	16.8	21.0	0.9	0.9	0.9
$\overline{B_s} \to K^{0*} \pi^0$	II	0.10	0.003	0.29	0.10	0.002	0.29	−1.7	−36.3	0.1
$\overline{B_s} \to K^0 \rho^0$	II	0.35	0.04	1.11	0.37	0.07	1.17	6.8	93.8	5.3
$\overline{B_s} \to K^0 \omega$	II,VI	1.14	0.16	1.81	1.42	0.26	1.83	24.7	56.7	1.2
$\overline{B_s} \to \overline{K^0}^* \eta$	II,VI	0.16	0.13	0.44	0.22	0.21	0.55	38.4	58.2	24.9
$\overline{B_s} \to \overline{K^0}^* \eta'$	II,VI	0.08	0.02	0.16	0.10	0.05	0.20	33.6	131	21.7
$\overline{B_s} \to K^+ K^{-*}$	IV	3.05	3.39	4.12	5.03	5.61	6.86	64.7	65.3	66.4
$\overline{B_s} \to K^{+*} K^-$	IV	0.89	0.97	1.15	0.90	0.99	1.18	2.2	2.3	2.5
$\overline{B_s} \to \rho \eta$	V	0.08	0.11	0.25	0.08	0.12	0.25	1.0	1.0	0.8
$\overline{B_s} \to \rho \eta'$	V	0.08	0.11	0.24	0.08	0.11	0.24	1.0	1.0	0.8
$\overline{B_s} \to \omega \eta$	V	0.85	0.01	2.60	1.29	0.01	4.15	51.5	−1.4	59.9
$\overline{B_s} \to \omega \eta'$	V	0.84	0.01	2.56	1.28	0.01	4.09	51.5	−1.4	59.9
$\overline{B_s} \to \pi^0 \phi$	V	0.13	0.17	0.32	0.13	0.17	0.32	1.9	1.8	1.3
$\overline{B_s} \to \phi \eta$	VI	1.85	0.76	0.07	3.78	1.69	0.03	104	122	−53.5
$\overline{B_s} \to \phi \eta'$	VI	0.70	0.20	1.49	1.82	0.40	1.14	161	107	−23.5
$\overline{B_s} \to K^0 \overline{K^0}^*$	IV	3.24	4.11	6.17	5.52	6.85	9.93	70.6	66.7	61.0
$\overline{B_s} \to K^{0*} \overline{K^0}$	IV	0.39	0.31	0.18	0.40	0.32	0.19	0.8	0.9	1.0
$\overline{B_s} \to K^0 \phi$	VI	0.001	0.03	0.30	0.004	0.03	0.40	118	1.1	38.4
$\overline{B_s} \to K^{+*} \rho^-$	I	12.5	14.1	17.5	12.6	14.2	17.7	0.9	0.9	0.9
$\overline{B_s} \to K^{0*} \rho^0$	II	0.29	0.03	0.94	0.31	0.06	0.99	6.8	93.8	5.3
$\overline{B_s} \to K^{0*} \omega$	II,VI	0.24	0.03	0.38	0.30	0.05	0.39	24.7	56.7	1.2
$\overline{B_s} \to K^{+*} K^{-*}$	IV	2.72	3.02	3.68	4.48	5.00	6.12	64.7	65.3	66.4
$\overline{B_s} \to \rho^0 \phi$	V	0.15	0.21	0.45	0.15	0.21	0.46	1.0	0.99	0.8
$\overline{B_s} \to \omega \phi$	V	0.79	0.01	2.41	1.20	0.01	3.85	51.3	−1.35	59.9
$\overline{B_s} \to K^{0*} \overline{K^0}^*$	IV	2.14	2.71	4.07	3.65	4.53	6.56	70.7	66.8	61.1
$\overline{B_s} \to K^{0*} \phi$	VI	0.03	0.12	0.48	0.05	0.19	0.74	68.5	58.9	54.1
$\overline{B_s} \to \phi \phi$	VI	17.5	8.99	0.42	29.9	15.8	0.98	71.1	75.8	134

TABLE IV. $\mathcal{B}(B_s \to PV, VV)$ (in units of 10^{-6}) in the SM and model III by using the LCSR form factors for $B_s \to K^*$ or $B_s \to \phi$ transition, and assuming $k^2 = m_b^2/2$, $\rho = 0.16$, $\eta = 0.34$, $M_{H^+} = 200$ GeV, $\theta = 0°$, and $N_c^{\rm eff} = 2$, 3, ∞.

		SM: $\mathcal{B}$			Model III: $\mathcal{B}$ and $\delta\mathcal{B}$ [%]					
Channel	Class	2	3	∞	2	3	∞	2	3	∞
$\overline{B}_s \to K^{*+}\pi^-$	I	4.68	5.29	6.61	4.69	5.29	6.61	0.0	0.0	0.0
$\overline{B}_s \to K^+\rho^-$	I	15.4	17.4	21.7	15.5	17.5	21.9	0.9	0.9	0.9
$\overline{B}_s \to K^{0*}\pi^0$	II	0.12	0.003	0.33	0.11	0.002	0.33	-1.7	-36.3	0.1
$\overline{B}_s \to K^0\rho^0$	II	0.36	0.04	1.16	0.39	0.07	1.22	6.8	93.8	5.3
$\overline{B}_s \to K^0\omega$	II,VI	1.19	0.17	1.89	1.49	0.27	1.91	24.7	56.7	1.2
$\overline{B}_s \to \overline{K}^{0*}\eta$	II,VI	0.18	0.14	0.50	0.24	0.22	0.62	36.7	57.8	23.6
$\overline{B}_s \to \overline{K}^{0*}\eta'$	II,VI	0.09	0.02	0.19	0.11	0.05	0.23	28.7	137	17.5
$\overline{B}_s \to K^+K^{-*}$	IV	3.22	3.58	4.35	5.31	5.92	7.22	64.7	65.3	66.4
$\overline{B}_s \to K^{+*}K^-$	IV	1.04	1.14	1.35	1.06	1.16	1.38	2.2	2.3	2.8
$\overline{B}_s \to \rho\eta$	V	0.09	0.12	0.26	0.09	0.12	0.26	1.0	1.0	0.8
$\overline{B}_s \to \rho\eta'$	V	0.09	0.12	0.25	0.09	0.12	0.25	1.0	1.0	0.8
$\overline{B}_s \to \omega\eta$	V	0.89	0.01	2.71	1.35	0.01	4.33	51.5	-1.4	59.9
$\overline{B}_s \to \omega\eta'$	V	0.88	0.01	2.67	1.33	0.01	4.27	51.5	-1.4	59.9
$\overline{B}_s \to \pi^0\phi$	V	0.26	0.33	0.63	0.26	0.34	0.64	1.9	1.8	1.3
$\overline{B}_s \to \phi\eta$	VI	1.36	0.49	0.18	3.04	1.23	0.09	124	151	-50.3
$\overline{B}_s \to \phi\eta'$	VI	0.38	0.53	3.43	0.87	0.21	2.91	127	-60.3	-15.3
$\overline{B}_s \to K^0\overline{K}^{0*}$	IV	3.42	4.34	6.52	5.83	7.23	10.5	70.6	66.7	61.0
$\overline{B}_s \to K^{0*}\overline{K}^0$	IV	0.46	0.37	0.22	0.46	0.37	0.22	0.8	0.9	1.0
$\overline{B}_s \to K^0\phi$	VI	0.004	0.05	0.36	0.002	0.05	0.50	-56.3	1.1	36.0
$\overline{B}_s \to K^{+*}\rho^-$	I	13.2	14.9	18.6	13.3	15.0	18.8	0.9	0.9	0.9
$\overline{B}_s \to K^{0*}\rho^0$	II	0.31	0.03	0.99	0.33	0.06	1.05	6.8	93.8	5.3
$\overline{B}_s \to K^{0*}\omega$	II,VI	0.26	0.04	0.40	0.32	0.06	0.41	24.7	56.7	1.2
$\overline{B}_s \to K^{+*}K^{-*}$	IV	2.82	3.13	3.79	4.64	5.17	6.33	64.7	65.3	66.4
$\overline{B}_s \to \rho^0\phi$	V	0.27	0.38	0.82	0.28	0.38	0.82	1.0	1.0	0.8
$\overline{B}_s \to \omega\phi$	V	1.43	0.01	4.33	2.16	0.01	6.93	51.5	-1.4	59.9
$\overline{B}_s \to K^{0*}\overline{K}^{0*}$	IV	2.20	2.80	4.20	3.76	4.67	6.77	70.7	66.8	61.1
$\overline{B}_s \to K^{0*}\phi$	VI	0.07	0.20	0.66	0.12	0.32	1.03	68.9	60.5	55.1
$\overline{B}_s \to \phi\phi$	VI	29.9	15.4	0.72	51.1	27.0	1.68	71.1	75.8	134

plot the mass and $N_c^{\rm eff}$ dependence of the branching ratios of $\overline{B}_s \to K^+K^-$ and $\eta\eta'$ decay modes.

After inclusion of new physics contributions in models I, II, and III, the patterns observed in Ref. [12] remain unchanged:

$$\Gamma(\overline{B}_s \to K^+K^-) > \Gamma(\overline{B}_s \to K^+K^{*-}) \gtrsim \Gamma(\overline{B}_s \to K^{*+}K^{*-}) > \Gamma(\overline{B}_s \to K^{+*}K^-),$$

$$\Gamma(\overline{B}_s \to K^0\overline{K}^0) > \Gamma(\overline{B}_s \to K^0\overline{K}^{*0}) \gtrsim \Gamma(\overline{B}_s \to K^{*0}\overline{K}^{*0}) > \Gamma(\overline{B}_s \to K^{*0}\overline{K}^0). \tag{49}$$

Recently, large decay rates for $B_u^+ \to K^+\eta'$ and $B_d \to K^0\eta'$ decays have been reported by the CLEO and BaBar Collaborations [4,5]. The CLEO measurement of $B_d^0 \to K^0\eta'$ decay is $\mathcal{B}(B_d^0 \to K^0\eta') = (89^{+18}_{-16} \pm 9) \times 10^{-6}$, which is larger than the branching ratios of $B \to K\pi$ decays by a factor of 3–5. For B_s decays, the decay modes $\overline{B}_s \to \eta\eta'$ and $\overline{B}_s \eta'\eta'$ are the analogue of $B_d \to K^0\eta'$ decay and are expected to have large branching ratios. From Table III, one can see that the SM predictions of the branching ratios $\mathcal{B}(B_s \to \eta\eta')$ and $\mathcal{B}(B_s \to \eta'\eta')$ are indeed large, but comparable in size with the other six decay modes listed in Eq. (48). The new physics enhancement to these two decay modes is significant in size, $\sim 70\%$ in model III, as illustrated in Fig. 3. After the inclusion of new physics contributions, we find numerically that

$$\mathcal{B}(\overline{B}_s \to \eta\eta') \approx (23\text{–}33) \times 10^{-6}, \tag{50}$$

$$\mathcal{B}(\overline{B}_s \to \eta'\eta') \approx (12\text{–}16) \times 10^{-6}. \tag{51}$$

TABLE V. $\mathcal{B}(B_s\to h_1 h_2)$ (in units of 10^{-6}) in model I, with $k^2=m_b^2/2$, $\rho=0.16$, $\eta=0.34$, $M_{H^+}=200$ GeV, $\tan\beta=2$, and $N_c^{\rm eff}=2,\quad 3,\quad \infty$.

		SM: $\mathcal{B}$			Model I: $\mathcal{B}$ and $\delta\mathcal{B}$ [%]					
Channel	Class	2	3	∞	2	3	∞	2	3	∞
$\overline{B}_s\to K i^+\pi^-$	I	6.33	7.13	8.88	6.34	7.14	8.90	0.1	0.1	0.1
$\overline{B}_s\to K^0\pi^0$	II	0.19	0.08	0.56	0.19	0.08	0.56	−0.1	0.0	0.1
$\overline{B}_s\to K^0\eta$	VI	0.34	0.31	0.78	0.34	0.31	0.79	0.4	0.7	0.4
$\overline{B}_s\to K^0\eta'$	VI	0.57	0.51	0.76	0.58	0.52	0.77	1.2	1.5	1.3
$\overline{B}_s\to K^+K^-$	IV	10.6	11.7	14.0	10.8	11.9	14.1	1.4	1.3	1.3
$\overline{B}_s\to\pi^0\eta$	V	0.04	0.06	0.11	0.05	0.06	0.11	10.5	10.0	7.3
$\overline{B}_s\to\pi^0\eta'$	V	0.04	0.05	0.10	0.05	0.06	0.11	10.5	10.0	7.3
$\overline{B}_s\to\eta\eta'$	VI	13.7	15.8	20.5	13.9	16.1	20.8	1.1	1.2	1.3
$\overline{B}_s\to\eta'\eta'$	VI	6.77	7.48	9.05	6.89	7.63	9.22	1.5	1.5	1.6
$\overline{B}_s\to\eta\eta$	VI	6.95	8.35	11.5	7.03	8.44	11.7	0.8	0.9	1.0
$\overline{B}_s\to K^0\overline{K^0}$	IV	11.4	13.2	17.2	11.6	13.4	17.5	1.8	1.9	2.0
$\overline{B}_s\to K^{*+}\pi^-$	I	4.04	4.56	5.70	4.04	4.56	5.70	0.0	0.0	0.0
$\overline{B}_s\to K^+\rho^-$	I	14.7	16.6	20.8	14.8	16.7	20.8	0.0	0.0	0.0
$\overline{B}_s\to K^{0*}\pi^0$	II	0.10	0.003	0.29	0.10	0.003	0.29	0.3	5.1	0.0
$\overline{B}_s\to K^0\rho^0$	II	0.35	0.04	1.11	0.35	0.04	1.11	0.0	0.5	0.0
$\overline{B}_s\to K^0\omega$	II,VI	1.14	0.16	1.81	1.15	0.17	1.81	0.6	1.3	0.0
$\overline{B}_s\to\overline{K^0}^*\eta$	II,VI	0.16	0.13	0.44	0.16	0.13	0.45	0.4	0.8	0.5
$\overline{B}_s\to\overline{K^0}^*\eta'$	II,VI	0.08	0.02	0.16	0.08	0.02	0.17	0.6	2.8	0.5
$\overline{B}_s\to K^+K^{-*}$	IV	3.04	3.38	4.11	3.12	3.45	4.18	2.1	1.9	1.5
$\overline{B}_s\to K^{+*}K^-$	IV	0.89	0.97	1.15	0.87	0.96	1.14	−1.5	−1.0	−0.2
$\overline{B}_s\to\rho\eta$	V	0.08	0.11	0.25	0.09	0.12	0.26	5.4	5.6	4.6
$\overline{B}_s\to\rho\eta'$	V	0.08	0.11	0.24	0.09	0.12	0.25	5.4	5.6	4.6
$\overline{B}_s\to\omega\eta$	V	0.85	0.01	2.59	0.86	0.01	2.65	0.8	−7.4	2.0
$\overline{B}_s\to\omega\eta'$	V	0.84	0.01	2.55	0.85	0.01	2.61	0.8	−7.4	2.0
$\overline{B}_s\to\pi^0\phi$	V	0.13	0.17	0.32	0.14	0.18	0.34	10.5	10.0	7.3
$\overline{B}_s\to\phi\eta$	VI	1.84	0.75	0.07	1.86	0.76	0.07	0.4	0.2	2.6
$\overline{B}_s\to\phi\eta'$	VI	0.69	0.20	1.49	0.71	0.20	1.51	1.0	0.0	1.2
$\overline{B}_s\to K^0\overline{K^0}^*$	IV	3.22	4.09	6.15	3.30	4.19	6.31	2.0	2.1	2.3
$\overline{B}_s\to K^{0*}\overline{K^0}$	IV	0.39	0.31	0.18	0.39	0.31	0.18	−0.4	−1.0	−2.9
$\overline{B}_s\to K^0\phi$	VI	0.001	0.03	0.30	0.002	0.03	0.30	0.3	2.1	1.7
$\overline{B}_s\to K^{+*}\rho^-$	I	12.4	14.1	17.5	12.5	14.1	17.5	0.0	0.0	0.0
$\overline{B}_s\to K^{0*}\rho^0$	II	0.29	0.03	0.94	0.29	0.03	0.94	0.0	0.5	0.0
$\overline{B}_s\to K^{0*}\omega$	II,VI	0.24	0.03	0.38	0.24	0.04	0.38	0.6	1.3	0.0
$\overline{B}_s\to K^{+*}K^{-*}$	IV	2.71	3.02	3.66	2.78	3.08	3.73	2.1	1.9	1.5
$\overline{B}_s\to\rho^0\phi$	V	0.15	0.21	0.45	0.16	0.22	0.47	5.4	5.6	4.6
$\overline{B}_s\to\omega\phi$	V	0.79	0.01	2.40	0.80	0.01	2.46	0.7	−7.4	2.0
$\overline{B}_s\to K^{0*}\overline{K^0}^*$	IV	2.13	2.70	4.06	2.17	2.77	4.17	2.0	2.1	2.3
$\overline{B}_s\to K^{0*}\phi$	VI	0.03	0.12	0.48	0.03	0.12	0.49	3.8	2.9	2.4
$\overline{B}_s\to\phi\phi$	VI	17.4	8.95	0.42	17.7	9.08	0.42	1.1	1.1	0.5

These theoretical predictions will be tested by future experimental measurements.

For the decays $\overline{B}\to K^+K^{-*}$ and $\overline{B}\to K^{+*}K^{-*}$, they have relatively large decay rates and weak M_{H^+} and $N_c^{\rm eff}$ dependence. In Figs. 4 and 5, we plot the mass and $N_c^{\rm eff}$ dependence of the branching ratios $\mathcal{B}(\overline{B_s}\to K^+K^{-*})$ and $\mathcal{B}(K^{+*}K^{-*})$. It is easy to see that the new physics contributions in the model III to these two class-IV decays are

TABLE VI. $\mathcal{B}(B_s \to h_1 h_2)$ (in units of 10^{-6}) in model II, with $k^2 = m_b^2/2$, $\rho = 0.16$, $\eta = 0.34$, $M_{H^+} = 200$ GeV, $\tan\beta = 2$, and $N_c^{\rm eff} = 2, 3, \infty$.

		SM: $\mathcal{B}$			Model II: $\mathcal{B}$ and $\delta\mathcal{B}$ [%]					
Channel	Class	2	3	∞	2	3	∞	2	3	∞
$\overline{B_s} \to K^+\pi^-$	I	6.33	7.13	8.88	6.29	7.09	8.84	−0.6	−0.6	−0.6
$\overline{B_s} \to K^0\pi^0$	II	0.19	0.08	0.56	0.18	0.07	0.55	−4.7	−13.4	−2.9
$\overline{B_s} \to K^0\eta$	VI	0.34	0.31	0.78	0.31	0.28	0.74	−7.5	−9.8	−5.2
$\overline{B_s} \to K^0\eta'$	VI	0.57	0.51	0.76	0.52	0.45	0.70	−9.5	−11.6	−9.1
$\overline{B_s} \to K^+K^-$	IV	10.6	11.7	14.0	9.58	10.5	12.5	−10.2	−10.4	−10.8
$\overline{B_s} \to \pi^0\eta$	V	0.04	0.06	0.11	0.05	0.06	0.11	10.5	10.0	7.3
$\overline{B_s} \to \pi^0\eta'$	V	0.04	0.05	0.10	0.05	0.06	0.11	10.5	10.0	7.3
$\overline{B_s} \to \eta\eta'$	VI	13.7	15.8	20.5	12.1	14.0	18.2	−11.7	−11.6	−11.4
$\overline{B_s} \to \eta'\eta'$	VI	6.77	7.48	9.05	5.94	6.56	7.91	−12.5	−12.7	−12.9
$\overline{B_s} \to \eta\eta$	VI	6.95	8.35	11.5	6.21	7.49	10.4	−10.9	−10.6	−9.9
$\overline{B_s} \to K^0\overline{K^0}$	IV	11.4	13.2	17.2	10.3	11.9	15.6	−11.9	−11.7	−11.4
$\overline{B_s} \to K^{*+}\pi^-$	I	4.04	4.56	5.70	4.04	4.56	5.70	0.0	0.0	0.0
$\overline{B_s} \to K^+\rho^-$	I	14.7	16.6	20.8	14.7	16.6	20.8	−0.2	−0.2	−0.2
$\overline{B_s} \to K^{0*}\pi^0$	II	0.10	0.003	0.29	0.10	0.003	0.29	0.8	16.5	0.0
$\overline{B_s} \to K^0\rho^0$	II	0.35	0.04	1.11	0.35	0.03	1.10	−1.1	−16.7	−1.0
$\overline{B_s} \to K^0\omega$	II,VI	1.14	0.16	1.81	1.09	0.15	1.80	−4.5	−10.3	−0.2
$\overline{B_s} \to \overline{K}^{0*}\eta$	II,VI	0.16	0.13	0.44	0.15	0.12	0.42	−7.3	−11.1	−4.7
$\overline{B_s} \to \overline{K}^{0*}\eta'$	II,VI	0.08	0.02	0.16	0.07	0.02	0.16	−4.7	−17.9	−2.9
$\overline{B_s} \to K^+K^{-*}$	IV	3.04	3.38	4.11	2.74	3.03	3.66	−10.3	−10.7	−11.2
$\overline{B_s} \to K^{+*}K^-$	IV	0.89	0.97	1.15	0.87	0.95	1.14	−2.0	−1.6	−0.8
$\overline{B_s} \to \rho\eta$	V	0.08	0.11	0.25	0.09	0.12	0.26	5.4	5.6	4.6
$\overline{B_s} \to \rho\eta'$	V	0.08	0.11	0.24	0.09	0.12	0.25	5.4	5.6	4.6
$\overline{B_s} \to \omega\eta$	V	0.85	0.01	2.59	0.77	0.01	2.33	−9.9	−7.4	−10.3
$\overline{B_s} \to \omega\eta'$	V	0.84	0.01	2.55	0.76	0.01	2.30	−9.9	−7.4	−10.3
$\overline{B_s} \to \pi^0\phi$	V	0.13	0.17	0.32	0.14	0.18	0.34	10.5	10.0	7.3
$\overline{B_s} \to \phi\eta$	VI	1.84	0.75	0.07	1.51	0.60	0.09	−18.3	−20.5	26.8
$\overline{B_s} \to \phi\eta'$	VI	0.69	0.20	1.49	0.55	0.21	1.60	−21.3	7.5	7.6
$\overline{B_s} \to K^0\overline{K}^{0*}$	IV	3.22	4.09	6.15	2.85	3.64	5.54	−12.0	−11.3	−10.1
$\overline{B_s} \to K^{0*}\overline{K^0}$	IV	0.39	0.31	0.18	0.39	0.31	0.18	−0.6	−1.3	−3.2
$\overline{B_s} \to K^0\phi$	VI	0.001	0.03	0.30	0.002	0.03	0.28	6.6	2.0	−6.6
$\overline{B_s} \to K^{+*}\rho^-$	I	12.4	14.1	17.5	12.4	14.0	17.5	−0.2	−0.2	−0.2
$\overline{B_s} \to K^{0*}\rho^0$	II	0.29	0.03	0.94	0.29	0.03	0.93	−1.1	−16.7	−1.0
$\overline{B_s} \to K^{0*}\omega$	II,VI	0.24	0.03	0.38	0.23	0.03	0.38	−4.5	−10.3	−0.2
$\overline{B_s} \to K^{+*}K^{-*}$	IV	2.71	3.02	3.66	2.43	2.70	3.27	−10.3	−10.7	−11.2
$\overline{B_s} \to \rho^0\phi$	V	0.15	0.21	0.45	0.16	0.22	0.47	5.4	5.6	4.6
$\overline{B_s} \to \omega\phi$	V	0.79	0.01	2.40	0.71	0.01	2.16	−10.0	−7.4	−10.3
$\overline{B_s} \to K^{0*}\overline{K}^{0*}$	IV	2.13	2.70	4.06	1.88	2.41	3.66	−12.1	−11.3	−10.2
$\overline{B_s} \to K^{0*}\phi$	VI	0.03	0.12	0.48	0.03	0.11	0.44	−10.0	−9.2	−8.8
$\overline{B_s} \to \phi\phi$	VI	17.4	8.95	0.42	15.2	7.75	0.33	−13.0	−13.8	−21.4

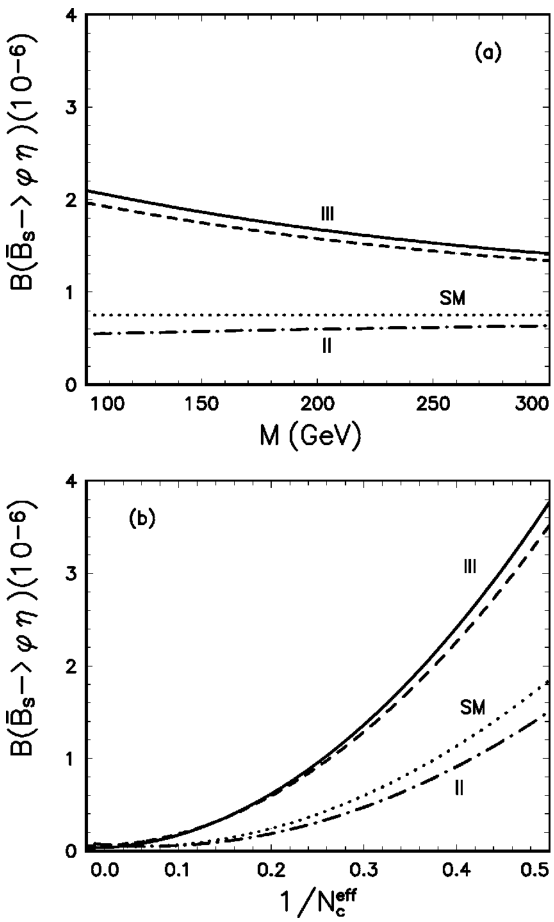

FIG. 1. Branching ratios $\mathcal{B}(\overline{B_s}\to\phi\eta)$ versus M_{H^+} and $1/N_c^{\rm eff}$ in the SM and models II and III by using the BSW form factors. For (a) and (b), we set $N_c^{\rm eff}=3$ and $M_{H^+}=200$ GeV, respectively. The four curves correspond to the theoretical predictions in the SM (dotted line), model II (dot-dashed curve), model III with $\theta=0°$ (solid curve), and $\theta=30°$ (short-dashed curve), respectively.

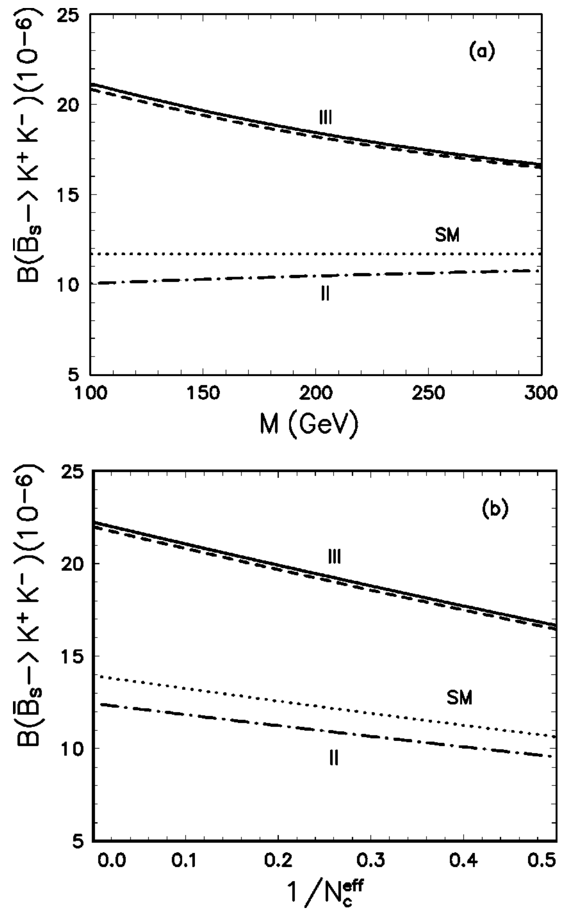

FIG. 2. Same as Fig. 1 but for the decay $\overline{B_s}\to K^+K^-$.

significant ($\sim$70%) in size and insensitive to the variations of M_{H^+} and $N_c^{\rm eff}$.

V. *CP*-VIOLATING ASYMMETRIES OF B_s MESON DECAYS

In Ref. [25], Du *et al.* studied the branching ratios and CP-violating asymmetries for decay modes $B_s\to K^-\pi^+$, K^+K^-, $\overline{K^0}\pi^0$, $\phi\phi$, and $\overline{K^0}\phi$. Recently, Ali *et al.* [42] estimated the CP-violating asymmetries in 76 charmless hadronic decays of B_u and B_d mesons. The calculation of the CP-violating asymmetry $\mathcal{A}_{CP}$ for B_s meson decays is theoretically very similar to that of the B_d meson decays. For more details about the theoretical aspects of CP-violating asymmetries in $B_{u,d}\to h_1h_2$ decays, one should see Ref. [42] and reference therein. In this section, we calculate the CP-violating asymmetries of $B_s\to h_1h_2$ decays in the framework of the SM and the general two-Higgs-doublet models. We focus on evaluating the new physics effects on $\mathcal{A}_{CP}$ for 39 B_s decay channels induced by charged-Higgs-boson penguin diagrams appearing in the general two-Higgs-doublet models.

In models I and II, one does not expect sizable changes in $\mathcal{A}_{CP}$ of B_s decays since there is no any new phase introduced when compared with the SM. In model III, although the introducing of a new phase θ played an important role in relaxing the constraint on the parameter space of model III due to the CLEO measurement of $B\to X_s\gamma$ decay as studied in Ref. [34], we still do not expect dramatic changes for the pattern of the CP-violating asymmetries of B_s decays under consideration because this phase may alter the theoretical prediction of $\mathcal{A}_{CP}$ through loop diagrams only.

Analogous to the B_d meson decays, the time-dependent CP asymmetry for the decays of states that were tagged as pure B_s^0 or $\overline{B_s^0}$ at production is defined as

$$\mathcal{A}_{CP}(t)=\frac{\Gamma(B_s^0(t)\to f)-\Gamma(\overline{B_s^0}(t)\to\overline{f})}{\Gamma(B_s^0(t)\to f)+\Gamma(\overline{B_s^0}(t)\to\overline{f})}. \tag{52}$$

Following Ref. [42], the neutral B_s^0 ($\overline{B_s^0}$) decays can be classified into three classes according to the properties of the final states f and $\overline{f}$.

(i) Class-1 decays: $B_s^0\to f$, $\overline{B_s^0}\to\overline{f}$, and the final states f or $\overline{f}$ is not a common final state of B_s^0 and $\overline{B_s^0}$, for example,

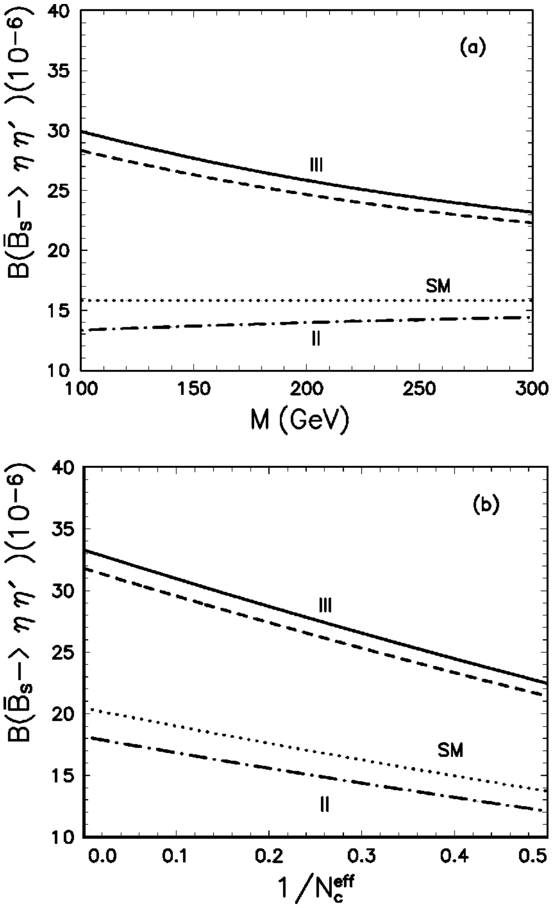

FIG. 3. Same as Fig. 1 but for the decay $\overline{B_s}\to\eta\eta'$.

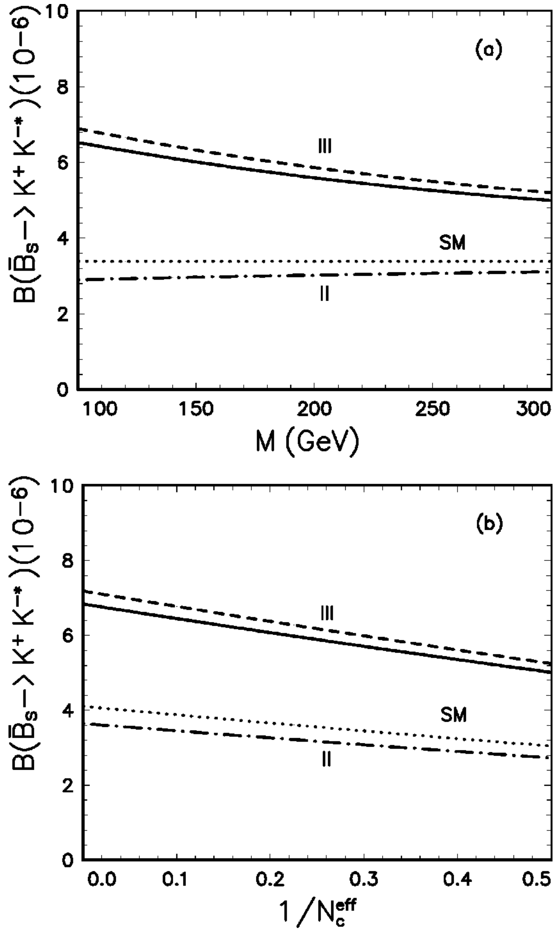

FIG. 4. Same as Fig. 1 but for the decay $\overline{B_s}\to K^+K^{-*}$.

$B_s^0\to K^+\pi^-$. The CP-violating asymmetry for class-1 decays will be independent of time,

$$\mathcal{A}_{CP}=\frac{\Gamma(B_s^0\to f)-\Gamma(\overline{B_s^0}\to\overline{f})}{\Gamma(B_s^0\to f)+\Gamma(\overline{B_s^0}\to\overline{f})}, \tag{53}$$

in terms of partial decay widths.

(ii) Class-2 and 3 decays: $\overset{(-)}{B}{}_s^0\to(f=\overline{f})$ with $f^{CP}=\pm f$ (class 2) or $f^{CP}\neq\pm f$ (class 3), the time-integrated CP asymmetries are of the form

$$\mathcal{A}_{CP}=\frac{1}{1+x^2}\,\frac{1}{1+|\lambda_{CP}|^2}-2\frac{x}{1+x^2}\,\frac{\mathrm{Im}(\lambda_{CP})}{1+|\lambda_{CP}|^2}, \tag{54}$$

with

$$\lambda_{CP}=\frac{V_{tb}^*V_{ts}}{V_{tb}V_{ts}^*}\,\frac{\langle f|H_{eff}|\overline{B_s^0}\rangle}{\langle f|H_{eff}|B_s^0\rangle}, \tag{55}$$

where $x=\Delta M_{B_s^0}/\Gamma_{B_s^0}\approx 20$ is the preferred value in the SM [25] for the case of B_s^0-$\overline{B_s^0}$ mixing.[3] Contrary to the B_d meson decay where $x\approx 0.73$, it is easy to see that the parameter x for B_s^0 decays is very large. The first and second terms in Eq. (54) are strongly suppressed by $1/x^2$ and $1/x$, respectively. We therefore do not expect large CP-violating asymmetries $\mathcal{A}_{CP}$ for the class-2 and class-3 B_s^0 decays. This expectation is confirmed by the numerical results given below.

In Tables VII and VIII, we present numerical results of CP-violating asymmetries $\mathcal{A}_{CP}$ for 39 $B_s\to h_1h_2$ decay channels in the SM and 2HDMs, using the input parameters as given in the Appendix and assuming that $k^2=m_b^2/2$, $\rho=0.16$, $\eta=0.34$, $M_{H^+}=200$ GeV, $\theta=0°,30°$, and $N_c^{\mathrm{eff}}=2$, 3, ∞. We show the numerical results for the case of using BSW form factors only since the differences induced by using the BSW or LCSR form factors are small for almost all B_s decay modes.

Among 39 B_s decay modes studied, we find that seven of them have CP-violating asymmetries larger than 20% in the SM and model III:

$$\overline{B_s}\to K^{0*}\pi^0, K^0\rho^0, \overline{K}^{0*}\eta^{(\prime)}, K^+K^{-*}, K^{0*}\rho^0, K^{0*}\omega. \tag{56}$$

[3] From Ref. [20], the upper limit is $x=\Delta M_{B_s^0}/\Gamma_{B_s^0}>15.7$ at 95% C.L.

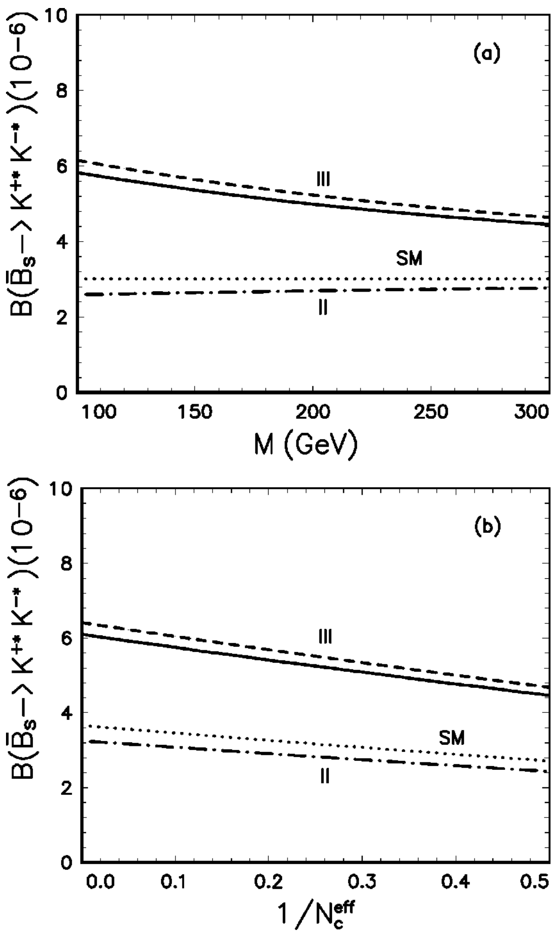

FIG. 5. Same as Fig. 1 but for the decay $\overline{B}_s \to K^{+*}K^{-*}$.

All these seven decay modes belong to the CP-class-1 decay modes. On the other hand, all 24 class-2 and -3 decay modes have small CP-violating asymmetries only, $|\mathcal{A}_{CP}| \lesssim 5\%$, mainly due to the strong suppression of $1/x^2$ as shown in Eq. (54).

In models I and II, the new physics corrections on $\mathcal{A}_{CP}$ for almost all B_s decay modes studied here are negligibly small as can be seen from Table VIII and Figs. 6–8. In model III, the new physics correction is varying from channel to channel, as illustrated in Table VII and Figs. 6–8: (i) For $\overline{B}_s \to K^+K^-$ decay, the new physics correction to its $\mathcal{A}_{CP}$ is very small in size and insensitive to the variations of $N_c^{\rm eff}$ and θ; (ii) for $\overline{B}_s \to K^+K^{-*}$ decay, the new physics correction to its $\mathcal{A}_{CP}$ is moderate in size, from -20% to -40% with $0° \leqslant \theta \leqslant 30°$, and insensitive to variations of $N_c^{\rm eff}$; (iii) for $\overline{B}_s \to \overline{K}^{0*}\eta'$ and three remaining decays given in Eq. (56), the size and the sign of the new physics corrections strongly depend on both $N_c^{\rm eff}$ and θ; (iv) for $\overline{B}_s \to \eta\eta', \phi\phi$ and several other CP class-2 and -3 decays, the new physics corrections can be as large as a factor of 30, but have a very strong dependence on $N_c^{\rm eff}$ and θ. Despite the large new physics correction to these decay modes, their $\mathcal{A}_{CP}$ are still smaller than 5% because of strong suppression of $1/x^2$.

For the QCD penguin-dominated $\overline{B}_s \to K^+K^{-*}$ decay, its decay amplitude is proportional to the combination of large and $N_c^{\rm eff}$ stable coefficients a_1 and a_4 [12]:

$$\mathcal{M}(\overline{B}_s \to K^+K^{-*}) \propto [V_{ub}V_{ts}^* a_1 - V_{tb}V_{ts}^*(a_4 + a_{10})]. \tag{57}$$

The imaginary parts of $\mathcal{M}$ for $b \to s$ and $\overline{b} \to \overline{s}$ transitions are very different, which in turn leads to a large A_{CP}. The numerical result indeed shows that this decay has a large and $N_c^{\rm eff}$ stable CP-violating asymmetry,

$$\mathcal{A}_{CP}(\overset{(-)}{B}_s \to K^{\pm}K^{\mp *}) \approx -30\% \tag{58}$$

for $2 \leqslant N_c^{\rm eff} \leqslant \infty$. Another advantage of this decay mode is the large ($\sim 70\%$) new physics enhancement to its branching ratio $\mathcal{B}(\overline{B}_s \to K^+K^{-*})$ in model III, as illustrated in Fig. 7. Taking into account the above facts, this decay mode $\overline{B}_s \to K^+K^{-*}$ seems to be the ''best'' channel to find CP violation of the B_s system through studies of two-body charmless decays of B_s meson.

Since the tree-dominated $\overline{B}_s \to K^+\pi^-$ decay mode has a moderate CP-violating asymmetry ($\sim 10\%$), a large branching ratio ($\sim 7 \times 10^{-6}$), negligible new physics correction, large detection efficiency,[4] and a very weak $N_c^{\rm eff}$ dependence, we therefore classify this decay mode as one of the promising decay channels for discovering the CP violation in B_s system.

For the decay $\overline{B}_s \to \overline{K}^{0*}\eta'$, although the SM prediction of its $\mathcal{A}_{CP}$ can be large, it is varying in the range of -60% to 60% due to the strong dependence on $N_c^{\rm eff}$, as illustrated in Fig. 8. Another disadvantage of this decay is its small branching ratio $(0.02–0.16) \times 10^{-6}$, almost two orders smaller than that of $\overline{B}_s \to K^+\pi^-$ and K^+K^{-*} decays.

For the remaining five decay modes as given in Eq. (56), although the size of their $\mathcal{A}_{CP}$ can also be as large as 20%–30%, but these decays can not be ''good'' channels for discovering the CP violation in the B_s system because of the strong $N_c^{\rm eff}$ dependence and very small branching ratios.

In Figs. 6 and 7, we show the mass and $N_c^{\rm eff}$ dependence of $\mathcal{A}_{CP}$ for $\overline{B}_s \to K^+K^-$ and K^+K^{-*} decays. In these figures, the dotted and dot-dashed curves refer to the theoretical prediction in the SM and model II, while the solid and short-dashed curves correspond to the prediction in the model III for $\theta = 0°$ and 30°, respectively. As can be seen from Fig. 7, the CP-violating asymmetry of $\overline{B}_s \to K^+K^{-*}$ decay is large in size and has weak or moderate dependence on M_{H^+}, $N_c^{\rm eff}$, and θ.

VI. SUMMARY AND DISCUSSIONS

In this paper, we calculated the branching ratios and CP-violating asymmetries of two-body charmless hadronic decays of B_s mesons in the standard model and the general

[4]In general, the detection efficiency for the two-body B meson decays with charged final states is larger than that with neutral final states by a factor of 2 or 3.

TABLE VII. CP-violating asymmetries $\mathcal{A}_{CP}(B_s \to h_1 h_2)$ (in percent) in the SM and model III, with $k^2 = m_b^2/2$, $\rho = 0.16$, $\eta = 0.34$, $M_{H^+} = 200$ GeV, $\theta = 0°, 30°$, and $N_c^{\rm eff} = 2$, 3, ∞.

		SM			Model III: $\theta = 0°$			Model III: $\theta = 30°$		
Channel	CP class	2	3	∞	2	3	∞	2	3	∞
$\overline{B_s} \to K^+ \pi^-$	1	10.2	10.2	10.3	9.95	9.96	9.97	10.2	10.2	10.3
$\overline{B_s} \to K_S^0 \pi^0$	2	−1.99	−3.98	4.50	−3.18	−3.87	4.48	−2.60	−4.51	4.36
$\overline{B_s} \to K_S^0 \eta$	2	−4.73	−3.62	2.93	−4.94	−3.59	2.17	−4.76	−4.19	1.67
$\overline{B_s} \to K_S^0 \eta'$	2	0.31	−2.86	−4.74	−0.50	−2.99	−4.96	−1.44	−3.84	−4.77
$\overline{B_s} \to K^+ K^-$	2	−1.71	−1.74	−1.77	−1.40	−1.41	−1.43	−2.38	−2.40	−2.45
$\overline{B_s} \to \pi^0 \eta$	2	−2.72	−0.24	2.93	−2.69	−0.24	2.92	−2.69	−0.24	2.92
$\overline{B_s} \to \pi^0 \eta'$	2	−2.72	−0.24	2.93	−2.69	−0.24	2.92	−2.69	−0.24	2.92
$\overline{B_s} \to \eta \eta'$	2	0.07	0.05	0.01	0.05	0.03	0.01	−1.08	−1.09	−1.11
$\overline{B_s} \to \eta' \eta'$	2	−0.16	0.03	0.36	−0.13	0.02	0.27	−1.34	−1.21	−0.98
$\overline{B_s} \to \eta \eta$	2	0.30	0.06	−0.31	0.24	0.05	−0.25	−0.81	−0.97	−1.24
$\overline{B_s} \to K^0 \overline{K^0}$	2	0.05	0.04	0.04	0.03	0.03	0.03	−1.19	−1.18	−1.17
$\overline{B_s} \to K^{*+} \pi^-$	1	0.34	0.34	0.34	0.34	0.34	0.34	0.34	0.34	0.34
$\overline{B_s} \to K^+ \rho^-$	1	5.56	5.56	5.55	5.52	5.51	5.51	5.60	5.60	5.59
$\overline{B_s} \to K^{0*} \pi^0$	1	−8.45	−26.6	6.17	−8.59	−41.2	6.17	−8.40	−40.1	6.27
$\overline{B_s} \to K_S^0 \rho^0$	1	−22.6	−16.3	15.5	−21.1	−7.99	14.8	−20.3	−16.6	15.4
$\overline{B_s} \to K_S^0 \omega$	2	3.88	−1.60	4.53	3.15	−2.01	4.65	2.78	−2.90	4.64
$\overline{B_s} \to \overline{K}^{0*} \eta$	1	−27.3	−0.36	23.1	−19.5	−0.01	18.6	−21.6	−4.60	18.7
$\overline{B_s} \to \overline{K}^{0*} \eta'$	1	52.8	30.8	−45.0	39.9	14.1	−36.7	42.5	−2.09	−35.7
$\overline{B_s} \to K^+ K^{-*}$	1	−30.5	−30.9	−31.7	−18.8	−19.0	−19.4	−23.9	−24.2	−24.6
$\overline{B_s} \to K^{+*} K^-$	1	1.40	1.45	1.53	1.37	1.42	1.49	1.37	1.41	1.49
$\overline{B_s} \to \rho \eta$	2	−3.03	−0.26	3.02	−3.02	−0.26	3.01	−3.02	−0.26	3.01
$\overline{B_s} \to \rho \eta'$	2	−3.03	−0.26	3.02	−3.02	−0.26	3.01	−3.02	−0.26	3.01
$\overline{B_s} \to \omega \eta$	2	−0.87	−1.01	−0.84	−0.71	−1.02	−0.68	−1.67	−1.02	−1.74
$\overline{B_s} \to \omega \eta'$	2	−0.87	−1.01	−0.84	−0.71	−1.02	−0.68	−1.67	−1.02	−1.74
$\overline{B_s} \to \pi^0 \phi$	2	−2.72	−0.24	2.93	−2.69	−0.24	2.92	−2.69	−0.24	2.92
$\overline{B_s} \to \phi \eta$	2	0.49	0.17	2.87	−0.71	−1.02	−0.68	−1.67	−1.02	−1.74
$\overline{B_s} \to \phi \eta'$	2	−0.31	0.25	−0.74	−0.71	−1.02	−0.68	−1.67	−1.02	−1.74
$\overline{B_s} \to K_S^0 \overline{K}^{0*}$	1	−1.25	−1.21	−1.13	−1.02	−0.98	−0.93	−6.98	−6.46	−5.72
$\overline{B_s} \to K^{0*} K_S^0$	1	−0.02	−0.03	−0.04	−0.02	−0.03	−0.04	−0.02	−0.03	−0.04
$\overline{B_s} \to K_S^0 \phi$	2	−3.38	−3.45	−3.27	−2.88	−3.45	−3.30	−4.42	−3.47	−3.84
$\overline{B_s} \to K^{+*} \rho^-$	1	5.56	5.56	5.55	5.52	5.51	5.51	5.60	5.60	5.59
$\overline{B_s} \to K^{0*} \rho^0$	1	−22.6	−16.3	15.5	−21.1	−7.99	14.8	−20.3	−16.6	15.4
$\overline{B_s} \to K^{0*} \omega$	1	25.5	13.1	5.43	20.6	8.57	5.37	20.9	4.39	5.46
$\overline{B_s} \to K^{+*} K^{-*}$	3	−3.86	−3.87	−3.90	−3.25	−3.27	−3.29	−4.05	−4.07	−4.10
$\overline{B_s} \to \rho^0 \phi$	3	−3.03	−0.26	3.02	−3.02	−0.26	3.01	−3.02	−0.26	3.01
$\overline{B_s} \to \omega \phi$	3	−0.87	−1.01	−0.84	−0.71	−1.02	−0.68	−1.67	−1.02	−1.74
$\overline{B_s} \to K^{0*} \overline{K}^{0*}$	3	0.05	0.05	0.04	0.04	0.03	0.03	−1.18	−1.13	−1.06
$\overline{B_s} \to K^{0*} \phi$	1	4.41	3.46	3.01	2.90	2.40	2.15	−3.03	−2.27	−1.91
$\overline{B_s} \to \phi \phi$	3	0.05	0.06	0.12	0.04	0.04	0.06	−1.19	−1.24	−1.79

two-Higgs-doublet models (models I, II, and III) by employing the NLO effective Hamiltonian with generalized factorization. In Sec. III, we defined the effective Wilson coefficients C_i^{eff} with the inclusion of new physics contributions, and presented the formulas needed to calculate the branching ratios $\mathcal{B}(B_s \to h_1 h_2)$.

In Sec. IV, we calculated the branching ratios for 39 $B_s \to h_1 h_2$ decays in the SM and models I, II, and III, presented

TABLE VIII. $\mathcal{A}_{CP}(B_s \to h_1 h_2)$ (in percent) in models I and II, with $k^2 = m_b^2/2$, $\rho = 0.16$, $\eta = 0.34$, $M_{H^+} = 200$ GeV, $\tan\beta = 2$, and $N_c^{\rm eff} = 2, 3, \infty$.

		SM			Model I			Model II		
Channel	CP class	2	3	∞	2	3	∞	2	3	∞
$\overline{B}_s \to K^+\pi^-$	1	10.2	10.2	10.3	10.2	10.3	10.3	10.3	10.3	10.3
$\overline{B}_s \to K_S^0\pi^0$	2	−1.99	−3.98	4.50	−1.98	−3.98	4.79	−1.63	−4.01	4.84
$\overline{B}_s \to K_S^0\eta$	2	−4.73	−3.62	2.93	−4.74	−3.62	2.92	−4.65	−3.63	3.11
$\overline{B}_s \to K_S^0\eta'$	2	0.31	−2.86	−4.74	0.28	−2.86	−4.75	0.52	−2.82	−4.64
$\overline{B}_s \to K^+K^-$	2	−1.71	−1.74	−1.77	−1.70	−1.72	−1.76	−1.80	−1.82	−1.86
$\overline{B}_s \to \pi^0\eta$	2	−2.72	−0.24	2.93	−2.59	−0.23	2.84	−2.59	−0.23	2.84
$\overline{B}_s \to \pi^0\eta'$	2	−2.72	−0.24	2.93	−2.59	−0.23	2.84	−2.59	−0.23	2.84
$\overline{B}_s \to \eta\eta'$	2	0.07	0.05	0.01	0.07	0.05	0.01	0.07	0.05	0.01
$\overline{B}_s \to \eta'\eta'$	2	−0.16	0.03	0.36	−0.16	0.03	0.36	−0.16	0.04	0.39
$\overline{B}_s \to \eta\eta$	2	0.30	0.06	−0.31	0.30	0.06	−0.31	0.31	0.06	−0.32
$\overline{B}_s \to K^0\overline{K}^0$	2	0.05	0.04	0.04	0.04	0.04	0.04	0.05	0.05	0.05
$\overline{B}_s \to K^{*+}\pi^-$	1	0.34	0.34	0.34	0.34	0.34	0.34	0.34	0.34	0.34
$\overline{B}_s \to K^+\rho^-$	1	5.56	5.56	5.55	5.57	5.57	5.56	5.58	5.57	5.57
$\overline{B}_s \to K^{0*}\pi^0$	1	−8.45	−26.6	6.17	−8.44	−25.3	6.18	−8.40	−22.9	6.18
$\overline{B}_s \to K_S^0\rho^0$	1	−22.6	−16.3	15.5	−22.6	−16.2	15.5	−22.9	−19.8	15.7
$\overline{B}_s \to K_S^0\omega$	2	3.88	−1.60	4.53	3.87	−1.62	4.53	4.03	−1.49	4.50
$\overline{B}_s \to \overline{K}^{0*}\eta$	1	−27.3	−0.36	23.1	−27.2	−0.36	23.1	−29.5	−0.50	24.3
$\overline{B}_s \to \overline{K}^{0*}\eta'$	1	52.8	30.8	−45.0	52.6	30.0	−44.8	55.4	37.1	−46.5
$\overline{B}_s \to K^+K^{-*}$	1	−30.5	−30.9	−31.7	−29.9	−30.4	−31.3	−33.9	−34.5	−35.6
$\overline{B}_s \to K^{+*}K^-$	1	1.40	1.45	1.53	1.43	1.47	1.53	1.44	1.47	1.54
$\overline{B}_s \to \rho\eta$	2	−3.03	−0.26	3.02	−2.96	−0.25	2.96	−2.96	−0.25	2.96
$\overline{B}_s \to \rho\eta'$	2	−3.03	−0.26	3.02	−2.96	−0.25	2.96	−2.96	−0.25	2.96
$\overline{B}_s \to \omega\eta$	2	−0.87	−1.01	−0.84	−0.87	−1.05	−0.84	−0.91	−1.05	−0.89
$\overline{B}_s \to \omega\eta'$	2	−0.87	−1.01	−0.84	−0.87	−1.05	−0.84	−0.91	−1.05	−0.89
$\overline{B}_s \to \pi^0\phi$	2	−2.72	−0.24	2.93	−2.59	−0.23	2.84	−2.59	−0.23	2.84
$\overline{B}_s \to \phi\eta$	2	0.49	0.17	2.87	−0.87	−1.05	−0.84	−0.91	−1.05	−0.89
$\overline{B}_s \to \phi\eta'$	2	−0.31	0.25	−0.74	−0.87	−1.05	−0.84	−0.91	−1.05	−0.89
$\overline{B}_s \to K_S^0\overline{K}^{0*}$	1	−1.25	−1.21	−1.13	−1.24	−1.20	−1.12	−1.31	−1.26	−1.18
$\overline{B}_s \to K^{0*}K_S^0$	1	−0.02	−0.03	−0.04	−0.02	−0.03	−0.04	−0.02	−0.03	−0.04
$\overline{B}_s \to K_S^0\phi$	2	−3.38	−3.45	−3.27	−3.39	−3.45	−3.27	−3.67	−3.45	−3.26
$\overline{B}_s \to K^{+*}\rho^-$	1	5.56	5.56	5.55	5.57	5.57	5.56	5.58	5.57	5.57
$\overline{B}_s \to K^{0*}\rho^0$	1	−22.6	−16.3	15.5	−22.6	−16.2	15.5	−22.9	−19.8	15.7
$\overline{B}_s \to K^{0*}\omega$	1	25.5	13.1	5.43	25.4	12.9	5.44	26.7	14.5	5.45
$\overline{B}_s \to K^{+*}K^{-*}$	3	−3.86	−3.87	−3.90	−3.83	−3.85	−3.89	−3.97	−3.99	−4.02
$\overline{B}_s \to \rho^0\phi$	3	−3.03	−0.26	3.02	−2.96	−0.25	2.96	−2.96	−0.25	2.96
$\overline{B}_s \to \omega\phi$	3	−0.87	−1.01	−0.84	−0.87	−1.05	−0.84	−0.91	−1.05	−0.89
$\overline{B}_s \to K^{0*}\overline{K}^{0*}$	3	0.05	0.05	0.04	0.05	0.05	0.04	0.06	0.05	0.05
$\overline{B}_s \to K^{0*}\phi$	1	4.41	3.46	3.01	4.28	3.38	2.96	4.81	3.74	3.25
$\overline{B}_s \to \phi\phi$	3	0.05	0.06	0.12	0.05	0.05	0.12	0.06	0.06	0.14

the numerical results in Tables III–VI, and displayed the M_{H^+} and $N_c^{\rm eff}$ dependence of several interesting decay modes in Figs. 1–5. From the numerical results, one can see the following.

(i) In models I and II, the new physics corrections to the decay rates of all $B_s \to h_1 h_2$ decay modes are small and will be masked by other larger known theoretical uncertainties.

(ii) In model III, the new physics corrections to QCD

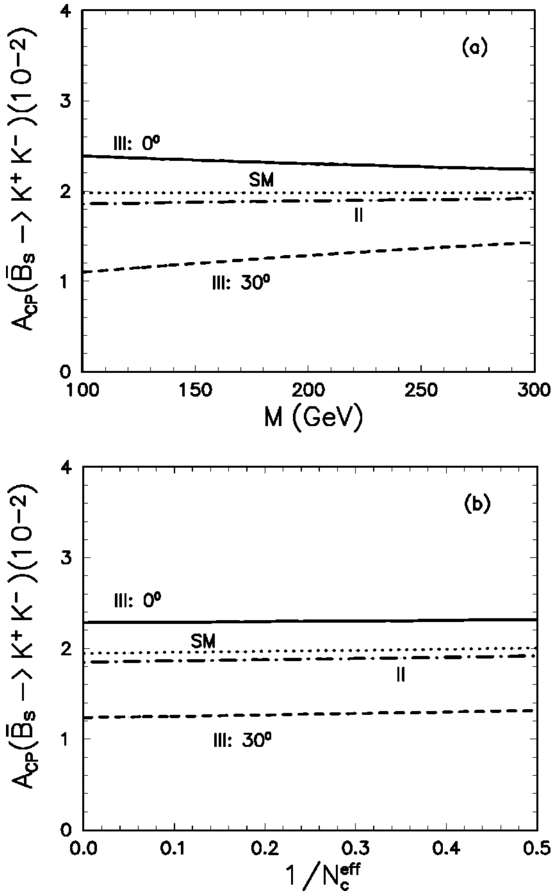

FIG. 6. CP-violating asymmetries A_{CP} of $\overline{B_s} \to K^+K^-$ decay versus M_{H^+} and $1/N_c^{\rm eff}$ in the SM and models II and III. For (a) and (b), we set $N_c^{\rm eff}=3$ and $M_{H^+}=200$ GeV, respectively. The four curves correspond to the theoretical predictions in the SM (dotted line), model II (dot-dashed curve), model III with $\theta=0°$ (solid curve), and $\theta=30°$ (short-dashed curve), respectively.

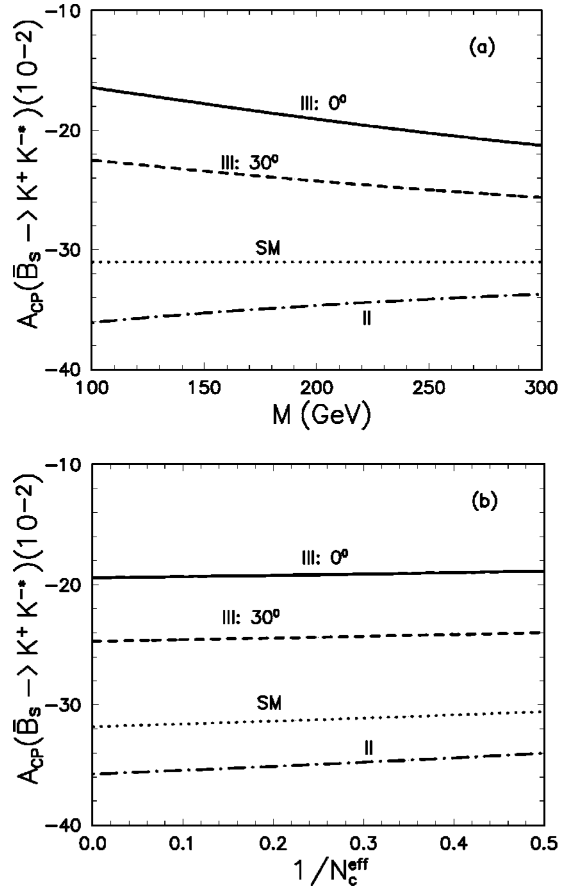

FIG. 7. Same as Fig. 6 but for decay $\overline{B_s} \to K^+K^-*$.

penguin-dominated decays $B_s \to K^0 \eta^{(\prime)}$, K^+K^-*, $\phi\phi$, etc., are large in size, from 30% to 130% with respect to the SM predictions, and insensitive to the variations of the mass M_{H^+} and $N_c^{\rm eff}$. For the tree- or electroweak penguin-dominated decay modes as listed in Eq. (46), however, the new physics corrections are very small in size: $\delta\mathcal{B} \leqslant 5\%$.

(iii) For the decays $\overline{B_s} \to \eta\eta'$ and $\overline{B_s} \to \eta'\eta'$, the analogue of $B_d \to K^0\eta'$ decay, the branching ratios are large but in comparable size with the other six decay modes listed in Eq. (48). The new physics enhancements to $\mathcal{B}(\overline{B_s} \to \eta\eta')$ and $\mathcal{B}(\overline{B_s} \to \eta'\eta')$ are significant in size, $\sim 70\%$ in model III.

(iv) For decay modes $B_s \to \pi^0\phi, \phi\eta', \rho^0\phi, \omega\phi$ and $B_s \to \phi\phi$, the variation of the branching ratios induced by using the BSW or LCSR form factors is about a factor of 2, but small or moderate for all other decay modes. This feature remains basically unchanged after the inclusion of new physics contributions.

(v) For $B_s \to K^+K^-$ and other decay modes as listed in Eq. (48), the branching ratios are at the level of $(1-3) \times 10^{-5}$ in the SM and model III. These decay modes will be measurable at the future hadron colliders with large b production.

In Sec. V, we calculated the CP-violating asymmetries $\mathcal{A}_{CP}$ for 39 $B_s \to h_1 h_2$ decays in the SM and 2HDMs, presented the numerical results in Tables VII and VIII, and displayed the M_{H^+} and $N_c^{\rm eff}$ dependence of $\mathcal{A}_{CP}$ for several typical decay modes in Figs. 6–8. From those tables and figures, the following conclusions can be drawn.

(i) For almost all B_s decay modes, the new physics corrections on $\mathcal{A}_{CP}$ are negligibly small in models I and II. In model III, the new physics correction is varying from channel to channel, and has a strong dependence on the parameter $N_c^{\rm eff}$ and the new phase θ for most decay modes.

(ii) For 24 CP-class-2 and -3 B_s meson decay modes, their CP-violating asymmetries are small, $|\mathcal{A}_{CP}| \leqslant 5\%$, due to the strong $1/x^2$ suppression.

(iii) Among the studied 39 B_s meson decay modes, seven of them can have a CP-violating asymmetry larger than 20% in magnitude.

(iv) The $\overline{B_s} \to K^+K^-*$ decay has a large and $N_c^{\rm eff}$- and θ-stable CP-violating asymmetry, $\approx -30\%$, and a large branching ratio. This mode seems to be the ''best'' channel to find CP violation of B_s system through studies of two-body charmless decays of B_s meson. The tree-dominated $\overline{B_s} \to K^+\pi^-$ decay is also a promising decay channel for discovering the CP violation in B_s system.

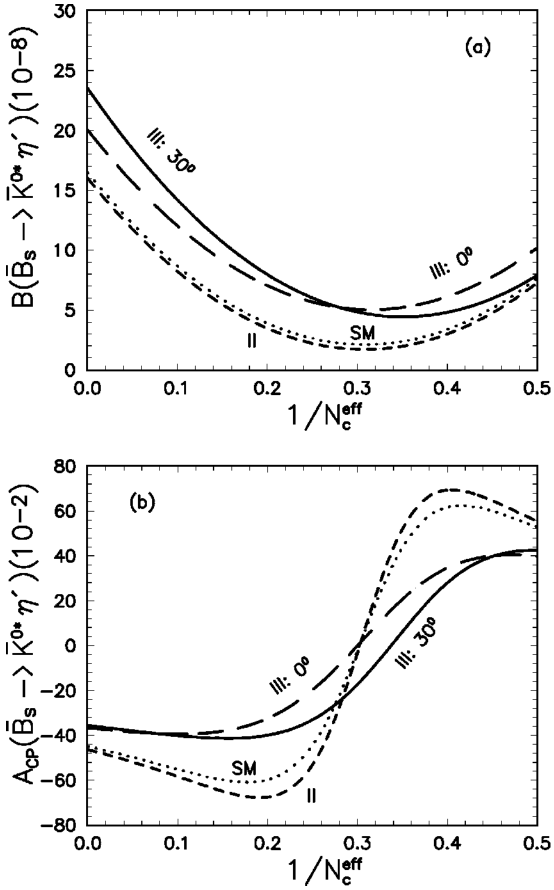

FIG. 8. Branching ratios and CP-violating asymmetries of $\overline{B_s} \to K^{0*}\eta'$ decay versus $1/N_c^{\rm eff}$ in the SM and models II and III, assuming $M_{H^+}=200$ GeV and $\tan\beta=2$. The four curves correspond to the theoretical predictions in the SM (dotted curve), model II (short-dashed curve), model III with $\theta=0°$ (long-dashed curve), and $\theta=30°$ (solid curve), respectively.

ACKNOWLEDGMENTS

The authors are very grateful to K.T. Chao, L.B. Guo, C.D. Lü, and Y.D. Yang for helpful discussions. C.S.L. acknowledges the support by the National Natural Science Foundation of China, the State Commission of Science and Technology of China, and the Doctoral Program Foundation of Institution of Higher Education. Z.J.X. acknowledges support of the National Natural Science Foundation of China under Grants No. 19575015 and 10075013, and the Excellent Young Teachers Program of Ministry of Education, China.

APPENDIX: INPUT PARAMETERS AND FORM FACTORS

In this appendix we present relevant input parameters. The input parameters are similar to those used in Ref. [12].

(i) The coupling constants, B meson masses, light meson masses, etc., are as follows (all masses in units of GeV) [12,20]:

$$\alpha_{em}=1/128, \quad \alpha_s(M_Z)=0.118, \quad \sin^2\theta_W=0.23,$$

$$G_F=1.16639\times 10^{-5}\ \ (\text{GeV})^{-2},$$

$$M_Z=91.188, \quad M_W=80.42, \quad m_{B_s^0}=5.369,$$

$$m_{\pi^\pm}=0.140,$$

$$m_{\pi^0}=0.135, \quad m_\eta=0.547, \quad m_{\eta'}=0.958,$$

$$m_\rho=0.770, \quad m_\omega=0.782,$$

$$m_\phi=1.019, \quad m_{K^\pm}=0.494, \quad m_{K^0}=0.498,$$

$$m_{K^{*\pm}}=0.892,$$

$$m_{K^{*0}}=0.896, \quad \tau(B_s^0)=1.493\ \text{ps}. \tag{A1}$$

(ii) For the elements of CKM matrix, we use Wolfenstein parametrization and fix the parameters A,λ,ρ,η to their central values:

$$A=0.804, \quad \lambda=0.22, \quad \rho=0.16, \quad \eta=0.34. \tag{A2}$$

(iii) Following Refs. [26,13], the current quark masses evaluated at the scale $\mu=m_b$ will be used in the numerical calculations:

$$m_b(m_b)=4.34\ \ \text{GeV}, \quad m_c(m_b)=0.95\ \ \text{GeV},$$

$$m_s(m_b)=0.105\ \ \text{GeV},$$

$$m_d(m_b)=6.4\ \ \text{MeV}, \quad m_u(m_b)=3.2\ \ \text{MeV}. \tag{A3}$$

For the mass of the heavy top quark we also use $m_t = \overline{m_t}(m_t)=168$ GeV.

(iv) For the decay constants of light mesons, the following values are used in the numerical calculations (in units of MeV):

$$f_\pi=133, \quad f_K=160, \quad f_{K^*}=221, \quad f_\rho=210,$$

$$f_\omega=195, \quad f_\phi=237,$$

$$f_\eta^u=f_\eta^d=78, \quad f_{\eta'}^u=f_{\eta'}^d=63, \quad f_\eta^c=-2.4,$$

$$f_{\eta'}^c=-6.3, \quad f_\eta^s=-112, \quad f_{\eta'}^s=137, \tag{A4}$$

where $f_{\eta^{(\prime)}}^u$ and $f_{\eta^{(\prime)}}^s$ have been defined in the two-angle-mixing formalism with $\theta_0=-9.2°$ and $\theta_8=-21.2°$ [43].

(v) In the calculation we use the following BSW form factors $F(0)$ (in the units of GeV) [25,16,12]:

$$F_0^{B\to\pi}(0)=0.33, \quad F_0^{B\to K}(0)=0.274,$$

$$F_0^{B\to\eta}(0)=-0.212, \quad F_0^{B\to\eta'}(0)=0.218,$$

$$A_{0,1,2}^{B\to\phi}(0)=0.273, \quad A_0^{B\to K^*}(0)=0.236,$$

$$A_{1,2}^{B\to K^*}(0)=0.232,$$

$$V^{B\to\phi}(0)=0.319, \quad V^{B\to K^*}(0)=0.2817. \tag{A5}$$

We use the monopole k^2 dependence for form factors,

$$f_i(k^2)=\frac{f_i(0)}{1-k^2/m_*^2}, \tag{A6}$$

where m_* is the pole mass given in [16]:

$$\{m(0^-),m(1^-),m(1^+),m(0^+)\} =\{5.2789,5.3248,5.37,5.73\} \tag{A7}$$

for $\overline{u}b$ and $\overline{d}b$ currents and

$$\{m(0^-),m(1^-),m(1^+),m(0^+)\}=\{5.3693,5.41,5.82,5.89\}, \tag{A8}$$

for $\overline{s}b$ currents.

(vi) For the decays involving $B_s\to K^*$ and $B_s\to\phi$ transitions, we also consider the case of using LCSR form factors with the k^2 dependence as defined in Ref. [44]:

$$f(k^2)=\frac{f(0)}{1-a(k^2/M_{B_s}^2)+b(k^2/M_{B_s}^2)^2}, \tag{A9}$$

where the values of $f(0)$ and coefficients a and b have been given in Ref. [44].

[1] *The BaBar Physics Book*, edited by P. F. Harrison and H. R. Quinn, Report No. SLAC-R-504, 1998.

[2] R. Fleischer and J. Matias, Phys. Rev. D **61**, 074004 (2000).

[3] CLEO Collaboration, Y. Gao and F. Würthwein, hep-ex/9904008, DPF99 Proceedings; CLEO Collaboration, M. Bishai *et al.*, Report No. CLEO CONF 99-13, hep-ex/9908018; CLEO Collaboration, T. E. Coan *et al.*, Report No. CLEO CONF 99-16, hep-ex/9908029; CLEO Collaboration, Y. Kwon *et al.*, Report No. CLEO CONF 99-14, hep-ex/9908039.

[4] CLEO Collaboration, S. J. Richichi *et al.*, Phys. Rev. Lett. **85**, 520 (2000).

[5] CLEO Collaboration, D. Cronin-Hennessy *et al.*, Phys. Rev. Lett. **85**, 515 (2000); CLEO Collaboration, C. P. Jessop *et al.*, *ibid.* **85**, 2881 (2000).

[6] BaBar Collaboration, J. Olson, talk presented at DPF 2000, 2000, BaBar Talk 00/27; BaBar Collaboration, F. Ferroni, talk presented at DPF 2000, 2000, BaBar Talk 00/12; BaBar Collaboration, B. Aubert *et al.*, BaBar-CONF-00-14, hep-ex/0008057.

[7] Belle Collaboration, A. Abashian *et al.*, contributed papers for ICHEP 2000, Belle-Conf-0005, Belle-Conf-0006, Belle-Conf-0007.

[8] H. Simma and D. Wyler, Phys. Lett. B **272**, 395 (1991); G. Kramer, W. F. Palmer, and H. Simma, Nucl. Phys. **B428**, 77 (1994); Z. Phys. C **66**, 429 (1995); R. Fleischer, Phys. Lett. B **321**, 259 (1994); Z. Phys. C **62**, 81 (1994); G. Kramer and W. F. Palmer, Phys. Rev. D **52**, 6411 (1995); N. G. Deshpande and X. G. He, Phys. Lett. B **336**, 471 (1994); G. Kramer, W. F. Palmer, and Y. L. Wu, Commun. Theor. Phys. **27**, 457 (1997); C.-W. Chiang and L. Wolfenstein, Phys. Rev. D **61**, 074031 (2000); T. Muta, A. Sugamoto, M. Z. Yang, and Y. D. Yang, *ibid.* **62**, 094020 (2000); M. Z. Yang and Y. D. Yang, *ibid.* **62**, 114019 (2000).

[9] D. Du and L. Guo, Z. Phys. C **75**, 9 (1997); J. Phys. G **23**, 525 (1997).

[10] A. Ali and C. Greub, Phys. Rev. D **57**, 2996 (1998); A. Ali, J. Chay, C. Greub, and P. Ko, Phys. Lett. B **424**, 161 (1998).

[11] A. Ali, G. Kramer, and C. D. Lü, Phys. Rev. D **58**, 094009 (1998).

[12] Y. H. Chen, H. Y. Cheng, and B. Tseng, Phys. Rev. D **59**, 074003 (1999).

[13] Y. H. Chen, H. Y. Cheng, B. Tseng, and K. C. Yang, Phys. Rev. D **60**, 094014 (1999).

[14] G. Buchalla, A. J. Buras, and M. E. Lautenbacher, Rev. Mod. Phys. **68**, 1125 (1996).

[15] A. J. Buras and R. Fleischer, in *Heavy Flavor II*, edited by A. J. Buras and M. Lindner (World Scientific, Singapore, 1998), p. 65; A. J. Buras, in *Probing the Standard model of Paticle Interactions*, edited by F. David and R. Gupta (Elsevier Science, British Vancouver, 1998).

[16] M. Bauer and B. Stech, Phys. Lett. **152B**, 380 (1985); M. Bauer, B. Stech, and M. Wirbel, Z. Phys. C **29**, 637 (1985); **34**, 103 (1987).

[17] H.-Y. Cheng, Phys. Lett. B **335**, 428 (1994); **395**, 345 (1997); H.-Y. Cheng and B. Tseng, Phys. Rev. D **58**, 094005 (1998).

[18] H.-Y. Cheng, Hsiang-nan Li, and K. C. Yang, Phys. Rev. D **60**, 094005 (1999).

[19] A. J. Buras and L. Silvestrini, Nucl. Phys. **B548**, 293 (1999).

[20] Particle Data Group, D. E. Groom *et al.*, Eur. Phys. J. C **15**, 1 (2000).

[21] L3 Collaboration, M. Acciarri *et al.*, Phys. Lett. B **363**, 127 (1995); ALEPH Collaboration, D. Buskulic *et al.*, *ibid.* **384**, 471 (1996).

[22] M. Beneke, G. Buchalla, C. Greub, A. Lenz, and U. Nierste, Phys. Lett. B **459**, 631 (1999), and references therein.

[23] DELPHI Collaboration, A. Abreu *et al.*, Eur. Phys. J. C **18**, 229 (2000); ALEPH Collaboration, R. Barate *et al.*, *ibid.* **7**, 553 (1999); OPAL Collaboration, G. Abbiendi *et al.*, *ibid.* **11**, 587 (1999).

[24] A. Deandrea, N. Di Bartolomeo, R. Gatto, and G. Nardulli, Phys. Lett. B **318**, 549 (1993); A. Deandrea, N. Di Bartolomeo, R. Gatto, F. Feruglio, and G. Nardulli, *ibid.* **320**, 170 (1993).

[25] D. S. Du and Z. Z. Xing, Phys. Rev. D **48**, 3400 (1993); D. S. Du and M. Z. Yang, Phys. Lett. B **358**, 123 (1995).

[26] B. Tseng, Phys. Lett. B **446**, 125 (1999).

[27] Z. J. Xiao, C. S. Li, and K. T. Chao, Phys. Rev. D **63**, 074005 (2001).

[28] S. Glashow and S. Weinberg, Phys. Rev. D **15**, 1958 (1977).

[29] D. Atwood, L. Reina, and A. Soni, Phys. Rev. D **55**, 3156 (1997).

[30] T. P. Cheng and M. Sher, Phys. Rev. D **35**, 3484 (1987); M.

Sher and Y. Yuan, *ibid.* **44**, 1461 (1991); W. S. Hou, Phys. Lett. B **296**, 179 (1992); A. Antaramian, L. J. Hall, and A. Rasin, Phys. Rev. Lett. **69**, 1871 (1992); L. J. Hall and S. Winberg, Phys. Rev. D **48**, R979 (1993); D. Chang, W. S. Hou, and W. Y. Keung, *ibid.* **48**, 217 (1993); Y. L. Wu and L. Wolfenstein, Phys. Rev. Lett. **73**, 1762 (1994); D. Atwood, L. Reina, and A. Soni, *ibid.* **75**, 3800 (1995); G. Cvetic, S. S. Hwang, and C. S. Kim, Phys. Rev. D **58**, 116003 (1998).

[31] M. Kabayashi and T. Maskawa, Prog. Theor. Phys. **49**, 652 (1973).

[32] F. M. Borzumati and C. Greub, Phys. Rev. D **58**, 074004 (1998); **59**, 057501 (1999).

[33] T. M. Aliev and E. O. Iltan, J. Phys. G **25**, 989 (1999).

[34] D. Bowser-Chao, K. Cheung, and W. Y. Keung, Phys. Rev. D **59**, 115006 (1999).

[35] Z. J. Xiao, C. S. Li, and K. T. Chao, Phys. Lett. B **473**, 148 (2000); Phys. Rev. D **62**, 094008 (2000).

[36] E. Gross, in the proceedings of EPS-HEP 99, Tampere, Finland, 1999.

[37] T. Inami and C. S. Lim, Prog. Theor. Phys. **65**, 297 (1981); **65**, 1772(E) (1981).

[38] Z. J. Xiao, L. X. Lü, H. K. Guo, and G. R. Lu, Eur. Phys. J. C **7**, 487 (1999); Z. J. Xiao, C. S. Li, and K. T. Chao, *ibid.* **10**, 51 (1999).

[39] H.-Y. Cheng and K. C. Yang, Phys. Rev. D **62**, 054029 (2000).

[40] J. Bijnens and F. Hoogeveen, Phys. Lett. B **283**, 434 (1992).

[41] R. Fleischer, Phys. Lett. B **332**, 419 (1994); N. G. Deshpande, X. G. He, and J. Trampetic, *ibid.* **345**, 547 (1995).

[42] A. Ali, G. Kramer, and Cai-Dian Lü, Phys. Rev. D **59**, 014005 (1999).

[43] T. Feldmann, P. Kroll, and B. Stech, Phys. Rev. D **58**, 114006 (1998).

[44] P. Ball and V. M. Braun, Phys. Rev. D **58**, 094016 (1998).